

CRYSTAL GROWTH OF SELECTED II-VI SEMICONDUCTING ALLOYS  
BY DIRECTIONAL SOLIDIFICATION

S. L. Lehoczky, F. R. Szofran, D. C. Gillies and S. D. Cobb  
NASA Marshall Space Flight Center

C.-H. Su and Y.-G. Sha  
Universities Space Research Association

R. N. Andrews  
University of Alabama at Birmingham

ABSTRACT

*A  $Hg_{0.84}Zn_{0.16}Te$  alloy crystal was back-melted and partially resolidified during the first United States Microgravity Laboratory (USML-1) mission in the Marshall Space Flight Center's Crystal Growth Furnace. The experiment was inadvertently terminated at about 30% of planned completion. Nonetheless, it was successfully demonstrated that HgZnTe alloy ingots partially grown and quenched on the ground can be back-melted and regrown in space under nearly steady state growth conditions. An identical "ground-truth" experiment was performed following the mission. Preliminary results are presented for both crystals, as well as for a series of other crystals grown prior to the mission for the purposes of optimizing in-flight growth conditions.*

INTRODUCTION

The growth of homogeneous crystals of mercury-based II-VI alloys, such as mercury zinc telluride ( $Hg_{1-x}Zn_xTe$ ,  $0 \leq x \leq 1$ ), from the melt is a particularly challenging problem because their liquidus and solidus temperatures (see for example Figure 1) are widely separated. Consequently, their interface segregation coefficient ( $k$ ) is large (Figure 2). Generally the density of the mercury compound is larger than the other II-VI alloying compound, e.g. ZnTe. This, when combined with the large change in the thermophysical properties upon phase change, makes the achievement and control of the desired solidification interface shape an extremely difficult task in a gravitational environment.

On Earth the Hg-rich component rejected during solidification is denser than the original melt and the vertical Bridgman-Stockbarger melt growth process would appear to be both gravitationally and thermally stable against convection. However, this is not generally the case. Due to the peculiar relationships between the thermal conductivities of the melt, solid, and ampoule, it is not practical to

completely avoid radial temperature gradients in the growth region for alloys of this type [1-4]. Because of the high Hg partial vapor pressures involved at the processing temperatures [5-8], the confinement of the alloys requires the use of very thick fused silica ampoules which have thermal conductivities compared to those of the alloys. This, when combined with the large (a factor of 4 to 10) decrease in the thermal conductivities of Hg-alloys upon freezing [9-11], leads to isothermal surfaces near the melt/solid interface that are bowed into the solid. Although the interface under this condition is neither an isothermal nor an isocompositional surface, it is bowed in the same direction as the adjacent isotherm. A method that relies on a careful control of radiation heat transfer near the growth interface can minimize this effect [1,4,12]; nonetheless, because the interface temperature undergoes large changes during growth, the complete elimination of radial temperature gradients in the vicinity of the interface is nearly impossible. Thus, in spite of the stabilizing influence of solutal density gradients, intense thermally-driven gravity-induced fluid flows will always occur near the interface [13-16]. Recent theoretical calculations [17] suggest that such flows should have only a small effect on the solidified alloy composition. On the other hand, alteration of the flow field by growth in a magnetic field yielded significant changes in the axial and radial compositional distribution in HgCdTe and HgZnTe alloys for the growth rates and temperature distributions employed [18]. One of the aims of this and other on-going flight experiments [19] is to evaluate the relative importance of various gravity and non-gravity related effects.

The specific objectives for the USML-1 phase of the investigation were:

1. To back melt a preprocessed  $\text{Hg}_{0.84}\text{Zn}_{0.16}\text{Te}$  solid solution alloy ingot and grow a 2 cm alloy crystal under nearly diffusion limited and stabilizing gravity conditions using a modified Bridgman growth method.
2. To establish whether preprocessed alloy crystals can be successfully quenched, back-melted, and regrown maintaining nearly steady-state compositions.
3. To freeze the diffusion boundary layer essentially without disturbing it, and from analysis of the boundary-layer composition to establish a value for the HgTe-ZnTe interdiffusion coefficient for the  $x=0.16$  alloy composition.
4. To perform detailed microstructural, electrical, and optical characterization on both the ground-grown and space-grown portion of the crystal, and evaluate the effects of reduced gravity for the USML-1 crystal growth conditions.
5. To perform detailed characterization of the rapidly frozen portions of the ingot to assess the potential benefits of casting alloy ingots in space.

The required duration time for the successful completion of the experiment was approximately 150 hours. Unfortunately, because of the loss of power to the Crystal Growth Furnace (CGF), the experiment was prematurely terminated at about 56 hours into the timeline. This significantly reduced the

science return of the experiment. Nonetheless, an approximately 5.7 mm-long crystal was grown during this time period. A summary of the results for the flight as well as the ground based portion of the experiment are described in the following sections.

## I. RESULTS FROM THE GROUND-BASED PORTION OF THE INVESTIGATION

A series of  $\text{Hg}_{0.84}\text{Zn}_{0.16}\text{Te}$  crystal ingots (Table 1) have been grown from pseudobinary melts by the Bridgman-Stockbarger type directional solidification using a MSFC/Space Science Laboratory (SSL) heat-pipe furnace [20] and the CGF Ground Control Experiment Laboratory (GCEL) furnace (Figure 3). A number of translation rates and a series of hot and cold zone temperatures were employed to assess the influence of growth parameters on crystal properties.

The ingots were sectioned longitudinally and transversely, polished, and etched appropriately to reveal macroscopic and microscopic defects including cracks, grain boundaries, voids, second-phase inclusions, and dislocations. Typically the ingots contained about  $2 \times 10^{-5}$  dislocations/cm<sup>2</sup> including dislocations that formed large numbers of sub-grain boundaries (Figure 4). An analysis of transmission electron micrographs (Figures 5 and 6) for selected wafers indicated the dislocation had 110-type Burger's vectors.

Precision mass density, wavelength-dispersive and energy-dispersive x-ray analyses were used to generate detailed compositional maps for the ingots. The fitting of the measured axial compositional variations to a one-dimensional diffusion model that includes changes in the interface temperature and segregation coefficient during the transient phase of solidification [21-24] was used to obtain an estimate for the effective HgTe-ZnTe liquid diffusion coefficient (D) and the fit for an x=0.18 alloy is shown in Fig. 7. A best estimate of  $D = 6.0 \times 10^{-6}$  cm<sup>2</sup>/s and the data in Figures. 1 and 2 were used to obtain  $G/R = 9.6 \times 10^{-6}$  °C-sec/cm<sup>2</sup> (G = temperature gradient in the melt ahead of the interface and R = solidification rate), the criterion for the prevention of interface breakdown resulting from constitutional supercooling. For optimum CGF operation conditions G was estimated to be about 35°C/cm, which allowed a maximum growth rate of about 3.8 mm/day. The time scale in Figure 7 illustrates the time consuming nature of growing significant lengths of crystals under steady state, and constant x conditions, and therefore the impossibility of meeting one of the major objectives within the 150 hours mission elapsed time allocated for the experiment. We decided therefore to grow the first part, the initial transient segment in Figure 7, of the crystal on the ground, and then rapidly freeze (quench) the remaining liquid to preserve the melt compositional distribution needed for the continuation of steady-state growth following back-melting on orbit. A series of growth runs was performed to establish the required protocols. Four precisely located thermocouples (See Figure 8) were used to establish the proper

back-melting position. The quench was initiated when the appropriate thermocouple read the solidus temperature of the  $x=0.16$  alloy, i.e., 695°C.

Figure 9 depicts the grain structure following a typical back-melting/regrowth sequence. As can be inferred from the figure, grain growth usually proceeded as would have been expected had there been no growth interruption. Figure 10 shows the behavior of the axial composition distribution prior to and after regrowths for one of the ingots. The data indicate that nearly steady state growth resumed following back melting without any significant composition transients.

Figure 11 and 12 show the interface region for two different temperature settings. As can be seen the melt/solid interface shapes are highly dependent on the exact temperature settings used. A hot zone temperature of 800°C and a cold zone temperature of 350°C were selected as optimum for the flight experiment. The radial compositional variations for the two cores are illustrated in Figures 13 and 14.

## II. FLIGHT AND GROUND-TRUTH SAMPLE RESULTS

### 1. USML-1 Experiment

The flight experiment on USML-1 was performed from June 26 to 28, 1992 on shuttle mission STS-50. Figure 15 shows the scheduled timeline for the experiment. The five-zone CGF illustrated in Figure 3 was heated to its set points in 5 hours and the furnace was translated at a rate of 10 mm/hr to the melt-back position as planned. After about 7.5 hours Process Elapsed Time (PET), the back-melting was completed, the furnace translation stopped and the sample was soaked for 10 hours before the directional solidification started at about 17.5 hours PET. The experiment was inadvertently terminated at 56.5 hours PET. The furnace lost its power and cooled in a passive mode. With a translation rate of 3.5 mm/day, a 5.7 mm long crystal was grown during the 39-hour growth period. A ground-truth growth experiment was performed after the flight mission using exactly the same timeline as the flight experiment including the power outage and the passive cool-down.

### 2. Sample Properties

#### a. Surface morphology

Figure 16 shows the radiograph of the returned flight sample and Figure 17 shows a flight sample inside the fused silica ampoule. The surface features before and after 4.7 cm from the sample tip are markedly different. From the quenched-in interface determined later, this position (4.7 cm) was the back-melt interface. As opposed to the sample grown on Earth, the portion of the sample melted in space showed partial separation from the ampoule wall. A scanning electron microscope (SEM)

photomicrograph of the surface of the space-grown region is shown in Figure 18 and the counterpart for the ground-truth sample is given in Figure 19.

*b. Quenched-in interface shape*

Figure 20 shows the quenched-in melt/solid interface in a longitudinal section cut from the flight sample. The interface was slightly concave toward the solid as was expected from previous ground based results. However, it was significantly more asymmetric when compared to the quenched-in interfaces seen for the GCEL samples. The sectioned area of the ground-truth sample shows more symmetric interface as depicted in Figure 21.

*c. Space-grown crystal microstructure*

A photomicrograph of the polished and etched slab from the flight sample is shown in Figure 22. The quenched-in interface can be easily seen and at 5.7 mm from this interface a discontinuity delineated by a concave boundary in the microstructure can also be observed. This boundary is believed to be the melt back interface. As shown in the figure, the space-grown crystal continued to grow in the same crystal orientation as the ground-grown part, and the first 2 to 3 mm crystal grown in space has a dense distribution of subgrain boundary structures which might have been caused by the applied thermal gradients and/or the abrupt changes in the local lattice constants due to the change in the axial composition as discussed later. However, when the crystal had grown to about 4 mm, as measured from the melt-back interface, the microstructure improved considerably with significant reduction in the density of subgrain boundaries, indicating that steady-state growth was nearly achieved. As can be seen an additional crystal grain was nucleated from the ampoule wall at about 2 mm from the melt-back interface.

*d. Radial compositional distribution of the grown crystals*

The radial compositional distributions at various axial locations were measured by using microprobe analysis. Figures 23 to 30 illustrate the sequence of the evolution of the radial composition distribution of the flight sample. The compositional distribution shown in Figure 26 is at an axial position of 6 mm in front of the quenched-in interface. The usual concave shape is distorted in the middle because only the central portion of the sample was back-melted due to the concavity. Figures 24 and 25 suggest that the initial resolidification phase passed through a transient period and, as shown in Figures 26 to 29, approached a steady-state growth about 3 mm from the quenched-in interface. This is consistent with the evolution of the microstructure shown in Figure 22. The asymmetry in the radial compositional profile at 1 mm in front of the quenched-in interface is also consistent with the asymmetry in the shape of the quenched-in interface. The asymmetry could have been caused by either an asymmetric temperature distribution or by residual transverse accelerations. Although we cannot completely rule out the first possibility, we believe that the more likely cause was residual transverse

accelerations. Data provided by the Orbital Acceleration Research Experiment (OARE) test project [25] tend to support this supposition. Although the residual acceleration along one of the transverse axes (Y) was about 0.15-0.2 $\mu$ g, as had been expected, along the other transverse axis (X), the measured accelerations were a factor of 2 to 3 larger and varied with time. As shown in Figure 31 as a function of mission elapsed time, these accelerations ranged from 0.4 to about 0.8 $\mu$ g. We have indicated in the figure the estimated times at which the growth translation started, as well as, when the growth interface was at various positions (5, 4, ... 1 mm) as measured from the quenched-in interface location. There appears to be a definite one-to-one correlation between the development of the compositional asymmetries shown in Figs. 24-28 and the changes in the magnitude of the residual acceleration X-component.

A rough estimate of the relative diffusion-limited radial segregation ( $\Delta C/C_0$ ) resulting from non-planar interface geometries may be obtained as described in Figure 32. The measured and estimated values for  $\Delta C/C_0$  and  $\Delta C_2/C_0$  corresponding to the quenched-in interface geometry are summarized in Table 2. The fact that the experimental values are 4 to 6 times larger than these estimated is not consistent with the assumption of purely diffusive mass transport.

The radial compositional distributions in the "ground-truth" sample are shown in Figures 33 to 37. Similar to the flight sample, the compositional distributions suggest a transient region followed by near steady state growth. Consistent with its interface shape, the radial composition distribution was highly asymmetric at 1 mm from the quenched-in interface. The relative radial segregation based on diffusive mass transfer was estimated to be 0.05 versus the measured value of about 0.18, suggesting significant flow contribution to the overall mass transfer process.

*e. Axial compositional distribution of the grown crystals*

The axial compositional variations along the grown crystal were measured by energy dispersive x-ray spectroscopy (EDS) on the sample surface as well as along the centerline of the ingot by microprobe, and are illustrated in Figures 38 and 39. The surface compositional profile shows an initial increase in the ZnTe mole fraction and then a gradual decrease to a steady state value. The centerline data were somewhat scattered and such a trend is not as clear. From the surface compositional profile and the radial compositional distributions shown in Figures 23 to 30, a slight excessive back-melting of 0.5 mm is estimated. Figures 40 and 41 show the similar data along the surface and the centerline, respectively, for the "ground-truth" sample. For both cases in the measurements of the "ground-truth" sample, an initial increase and a gradual decrease in the ZnTe mole fraction is indicated; suggesting slightly excessive back-melting.

#### *f. Microstructure of the quenched-in sections*

The quenched-in section of the flight sample was polished, etched and examined by the SEM using the back scattering mode. The back scattering photomicrographs of the quenched-in section of the flight sample (Figure 41) clearly show an array of long parallel dendritic structures originating at the quenched-in interface and extending into the melt at an angle of about 50 to 60° from the growth axis. This lack of symmetry is consistent with the observed asymmetries in the interface shape and in the radial compositional distribution. A similar micrograph for the "ground-truth" sample is shown in Figure 42. The major dendritic structures near the interface were rather short compared to the flight case, and show a nearly symmetric distribution about the growth axis as was the case for the radial compositional distribution.

#### *g. Axial compositional distribution in the quenched-in sections*

The axial compositions along the centerline of the flight sample in the quenched-in section were measured by microprobe and are plotted in Figure 44. The large fluctuation in the data is caused by the dendritic nature of the sample. Subsequently, the sample was annealed at 580°C for 114 hours and the composition distribution re measured and is shown in Figure 45. The annealing time and temperature were chosen to accelerate local diffusion between the dendritic core (high ZnTe content) and the last to freeze section (high HgTe content) while minimizing the effect on the axial compositional distribution. As expected, the annealing procedure greatly reduced the data scatter. The results show an initial increase in the mole fraction of ZnTe to a steady value of about 0.05. The axial data for the ground-truth sample for the as-quenched and the annealed cases are given in Figures 46 and 47, respectively. The data were taken 2 mm from the centerline to avoid large shrinkage cavities. The as-quenched sample shows much larger scatter than that of the flight sample. This is probably the result of the differences in the dendritic structure in the two cases. The profile for the annealed "ground-truth" sample is similar to that of the flight sample except the steady-state composition is somewhat higher.

Repeated annealing of the quenched samples generally resulted in an increase in the size of the larger shrinkage cavities and a reduction of the size of the smaller ones. This interesting behavior seems to provide strong evidence for the importance of a surface-energy driven ripening effect for the moderate temperatures and short time intervals used.

A back scattering micrograph of the very top portion of the as-quenched ground-truth sample is shown in Figure 48. The presumed high ZnTe content in the several bright areas seen in the figure was confirmed by EDS analysis which indicated a ZnTe content of over 60%. It is believed that during the rather slow cooling process a significant portion of the solid particles of high ZnTe content that formed in the melt just in front of the freezing interface floated to the top of the sample. As expected, no such areas of high ZnTe content were found in the top portion of the flight sample.

### **III. Summary of Preliminary Flight Results**

Because of the loss of power to the CGF, the experiment was terminated after approximately 39 hours into the growth period. About 5.7 mm of sample had been grown at that point. X-ray radiographs of the returned cartridges did not show any features for either the primary or the secondary (not heated in orbit) sample that indicated off-nominal behavior. It is very likely, therefore, that the experiment would have met its objectives for this mission if it had proceeded to conclusion.

Detailed surface photomicrographs of the removed sample clearly showed significant topographical differences between the space- and ground-grown portions. Measurements of the Zn content of the sample along the growth direction indicated that the back melting portion of the experiment was successfully accomplished as planned. The meltback interface location was within 0.5 mm of the desired value. Compositional measurements along the sample axis indicated that the desired steady-state growth for the axial composition was reached at about 3 mm into the growth. An X-ray diffraction and SEM survey of the sample showed that both the ground- and flight-portions of the ingot contained only a few grains, i.e., were nearly single crystals, and the crystallographic orientation was maintained following back-melting and space growth. The interface shape, radial compositional variations, and the quenched-in dendritic structures of the flight sample all have shown an asymmetric behavior. At least the compositional data strongly suggest that the most likely cause was unanticipated transverse residual accelerations.

### **ACKNOWLEDGMENTS**

We would like to thank R. K. Crouch and J. Kearns of NASA/HQ and D. A. Schaefer of NASA/MSFC for programmatic support, J. Mark Jones, NASA/MSFC for sample preparation, Greg Jerman for electron microprobe analysis and Shirley A. Buford, NASA/MSFC, for typing the manuscript for publication. We are also grateful to Robert E. Blanchard of NASA/LeRC for providing his OARE data prior to publication, and C. R. Baugher of NASA/MSFC and to the ACAP project for acceleration data reduction. The work was supported by the Microgravity Science and Applications Division of NASA

## REFERENCES

1. Szofran, F.R., and Lehoczky, S.L., *J. Crystal Growth* 70, 349 (1984).
2. Naumann, R.J., and Lehoczky, S.L., *J. Crystal Growth* 61, 707 (1983).
3. Jasinski, J., Rohsenow, W.M. and Witt, A.F., *J. Crystal Growth* 61, 339 (1983).
4. Dakhoul, Y.M., Farmer, R., Lehoczky, S.L. and Szofran, F.R., *J. Crystal Growth* 86, 49 (1988).
5. Steininger, J., Strauss, A.J., and Brebrick, R.F., *J. Electrochem. Soc.* 117, 1305 (1970).
6. Steininger, J., *J. Electron. Mater.* 5, 299 (1976).
7. Kelly, J.D., Martin, B.G., Szofran, F.R., and Lehoczky, S.L., *J. Electrochem Soc.* 129, 2360 (1982).
8. Yu, T.C. and Brebrick, R.F., *J. Phase Equilibria* 13, 476 (1992).
9. Holland, L.R., and Taylor, R.E., *J. Vacuum Sci. Technol. A1*, 1615 (1983).
10. Su, C.-H., *J. Crystal Growth* 78, 51 (1986).
11. Szofran, F. R. and Lehoczky, S. L., *Bull. APS* 28,1313 (1983).
12. Cobb, S.D., Andrews, R.N., Szofran, F.R. and Lehoczky, S.L., *J. Crystal Growth*, 110, 415 (1991).
13. Lehoczky, S.L. and Szofran, F.R., NASA Technical Paper 2787 (December 1987).
14. Lehoczky, S.L. and Szofran, F.R., "Growth of Solid Solution Single Crystals," in *The Nation's Future Materials Needs*, International SAMPE Technical Conference Series, Lynch, T., Persh, J., Wolf, T., and Rupert N., eds., (SAMPE: Technical Conference, Arlington, Virginia, October 13-15, 1987).
15. Cobb, S. D., Szofran, F. R. and Lehoczky, S. L., "Growth Rate Dependence of the Radial Segregation in Directionally Solidified  $Hg_{1-x}Cd_xTe$  Alloys," MCG/West 10th Conference on Crystal Growth, Fallen Leaf Lake, California, June 7-10, 1988.16. Kim, D.H. and Brown, R.A., Massachusetts Institute of Technology, private communication, to be published in *J. Crystal Growth*.
17. Kim, F.H., Brown, R.A., *J. Crystal Growth* 114, 411 (1991).
18. Su, C.-H., Lehoczky, S.L., and Szofran, F.R., *J. Crystal Growth* 109, 392 (1991).
19. Experiment to be flown on the Second United States Microgravity Payload (USMP-2) mission.
20. Lehoczky, S.L., Szofran, F.R., and Martin, B.G., NASA CR-161598, (1980).
21. Clayton, J.C., NASA CR-162049, (1982).
22. Clayton, J.C., Davidson, M.C., Gillies, D.C., and Lehoczky, S.L., *J. Crystal Growth* 60, 374 (1982).
23. Andrews, R.N., Szofran, F.R. and Lehoczky, S.L., *J. Crystal Growth*, 92, 445 (1988).

24. Szofran, F.R., Chandra, D., Wang, J.-C., Cothran, E.K., and Lehoczky, S.L., J. Crystal Growth 70, 343 (1984).
25. Blanchard, R.E. and Baugher, C.R., private communication (to be published).

**Table 1: Ground-Based  $\text{Hg}_{0.84}\text{Zn}_{0.16}\text{Te}$  Alloy Crystals Grown**

Sample	Preprocessed Furnace	Growth Furnace	Hot Zone Temp (°C)	Cold Zone Temp (°C)	Growth Rate (mm/day)	Length Grown (mm)
B16-L	SSL	-	790	530	3.8	101.3
*B18-K	SSL	SSL	790	550	3.8	29.6
+B16-1	SSL	GCEL (1)	800	375	3.5	10.8
		GCEL (2)	800	375	3.5	10.4
+B16-2	SSL	GCEL (1)	780	350	3.5	8.9
		GCEL (2)	780	350	3.5	11.6
+B164	SSL	GCEL (1)	800	555	3.5	21.7
		GCEL (2)	800	555	3.5	7.1
B16-8	GCEL	GCEL	800	350	3.5	17.7
B16-33	SSL	GCEL	800	350	3.5	17.9

\* $\text{Hg}_{0.82}\text{Zn}_{0.18}\text{Te}$  sample

+ For samples B16-1, 2 and 4, the samples were preprocessed in SSL furnace and back-melted, regrown, and quenched in GCEL (labeled as GCEL (1)), and then back-melted, and regrown again in GCEL (labeled as GCEL (2))

**Table 2: Measured and Estimated Radial Segregation**

Measured	Estimated
$\frac{\Delta C_1}{C_o} = 0.40$	$\frac{\Delta C_1}{C_o} = 0.068$
$\frac{\Delta C_2}{C_o} = 0.18$	$\frac{\Delta C_2}{C_o} = 0.046$

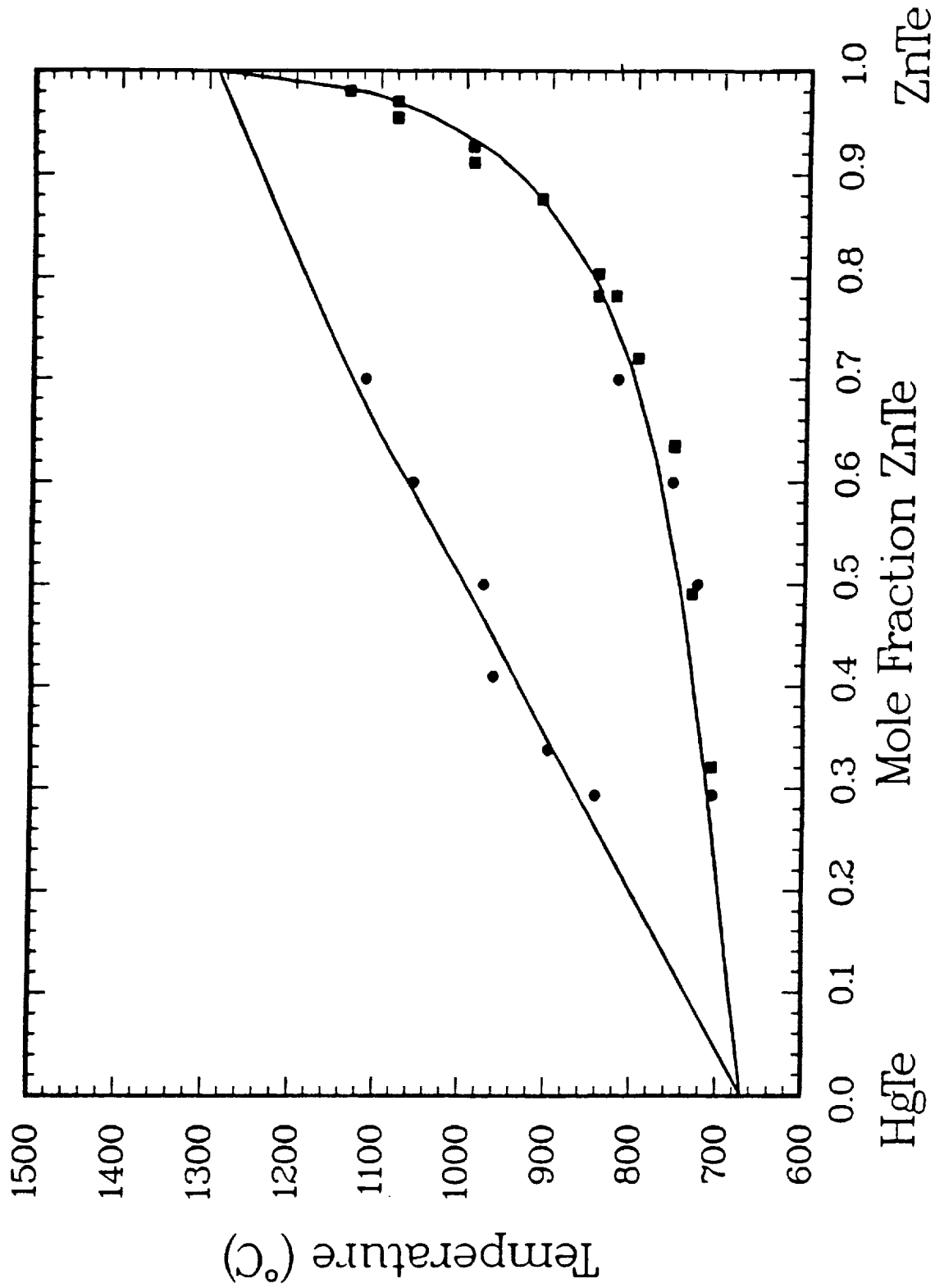


Figure 1  $\text{Hg}_{1-x}\text{Zn}_x\text{Te}$  pseudobinary constitutional phase diagram.

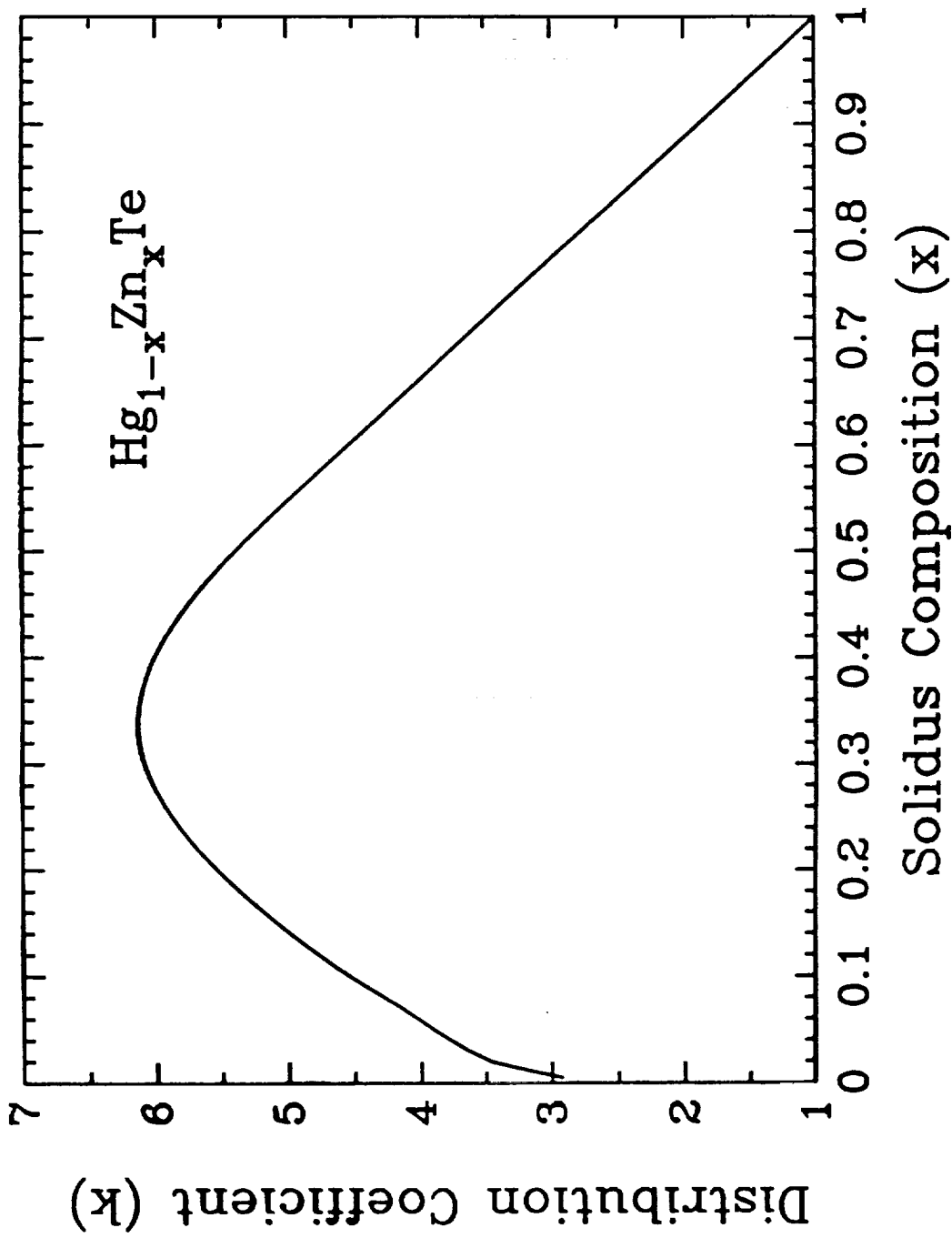
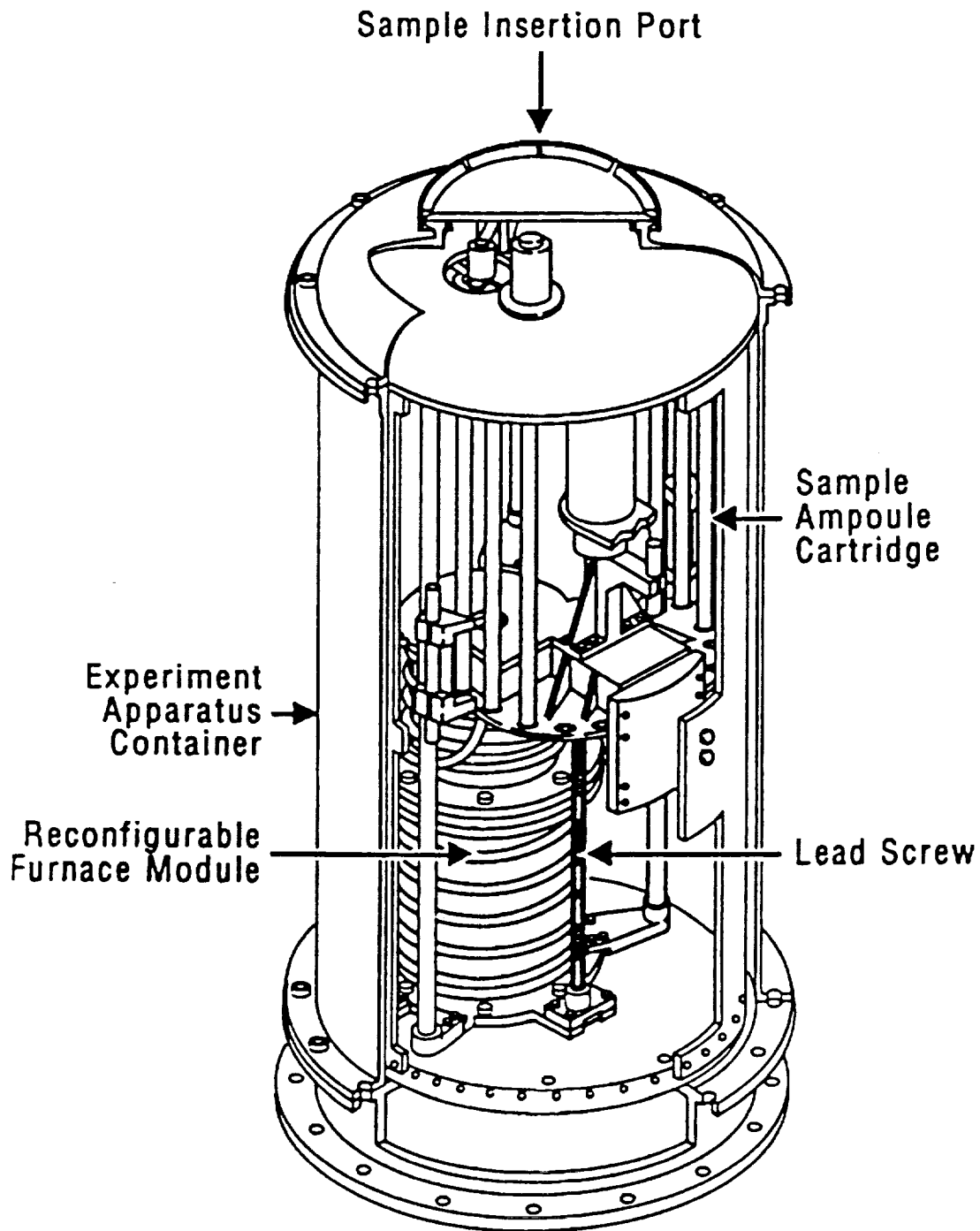


Figure 2 Composition dependence of the solidification interface segregation coefficient.



---

## The Crystal Growth Furnace

Integrated Furnace Experiment Assembly (IFEA)

Figure 3 Crystal Growth Furnace schematic

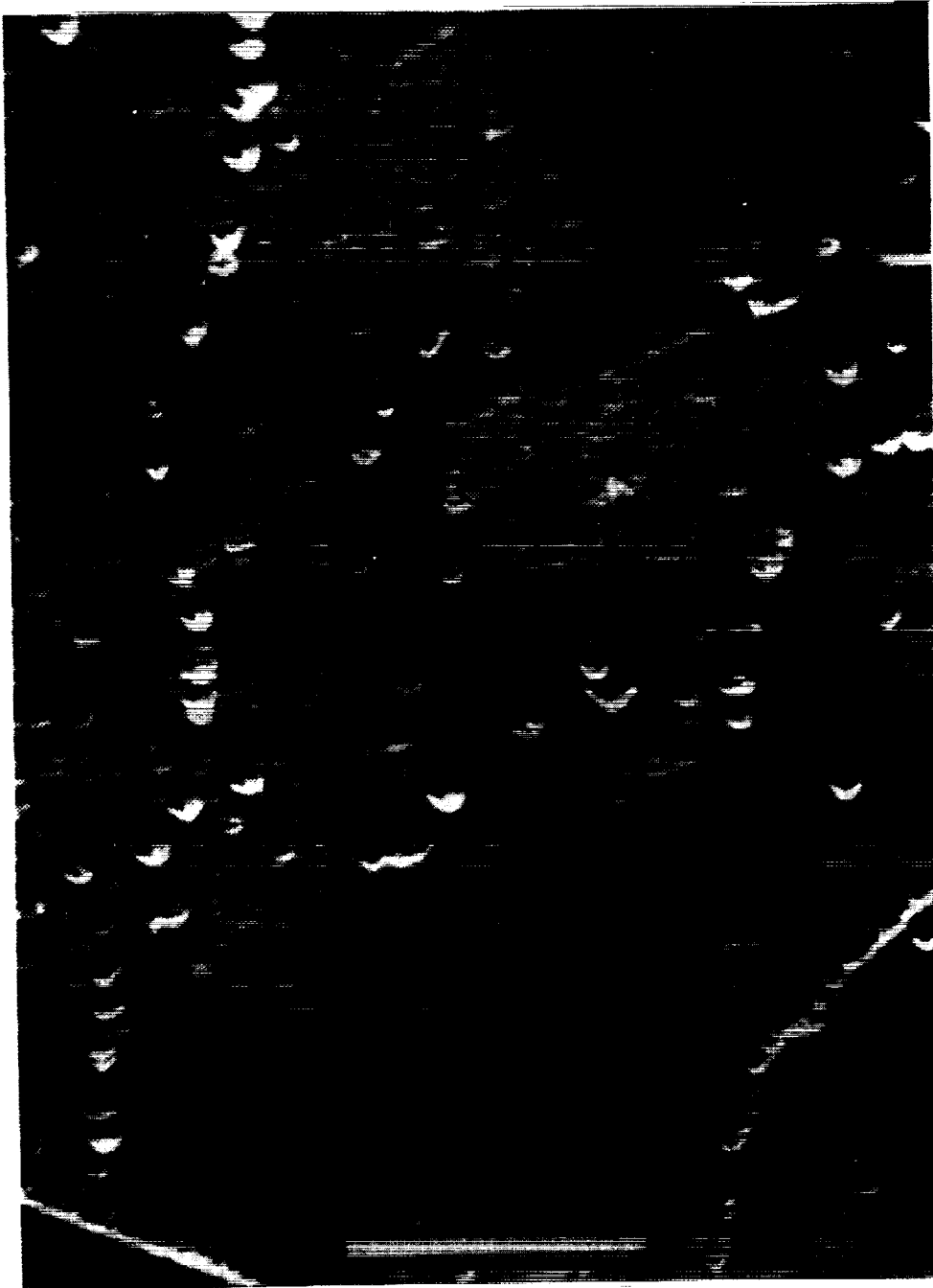


Figure 4 Typical dislocation etch pits showing individual dislocations and sub-grain boundaries. Marker represents 50  $\mu\text{m}$ .

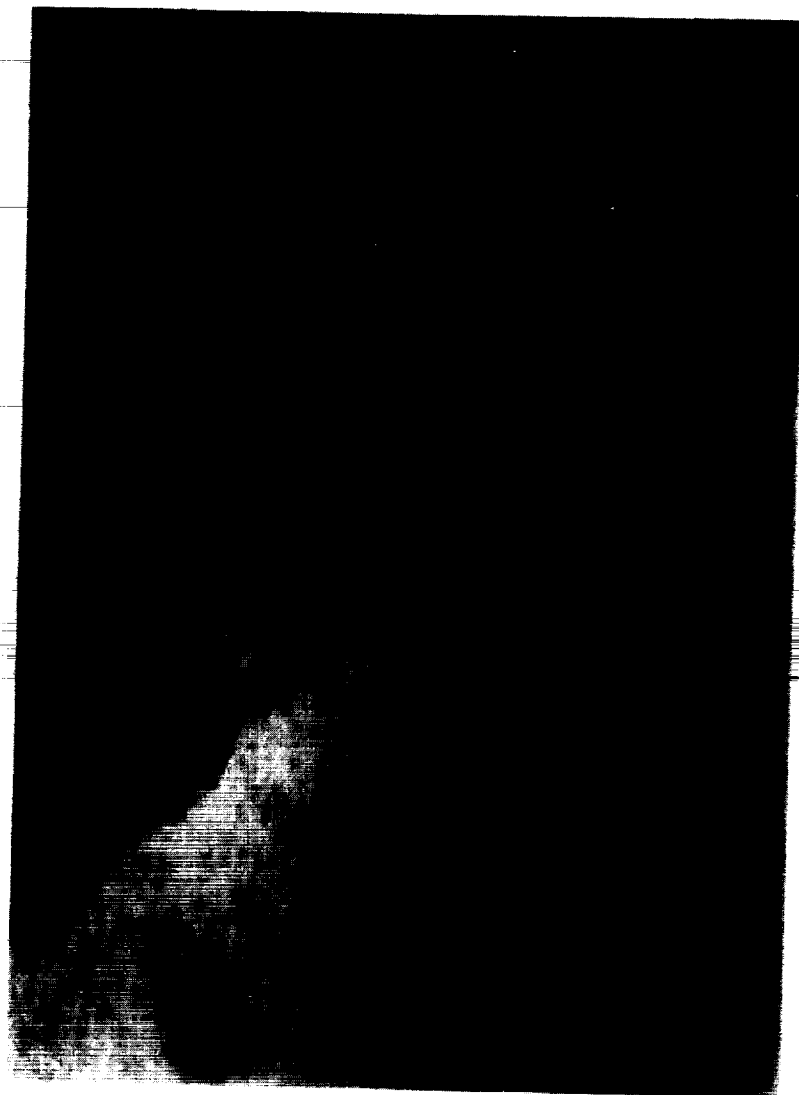


Figure 5 Transmission electron micrograph for a Hg<sub>0.84</sub>Zn<sub>0.16</sub>Te wafer showing a subgrain boundary.



Figure 6 Transmission electron micrograph for a  $\text{Hg}_{0.84}\text{Zn}_{0.16}\text{Te}$  wafer showing individual dislocations with 110-type Burger's vectors.

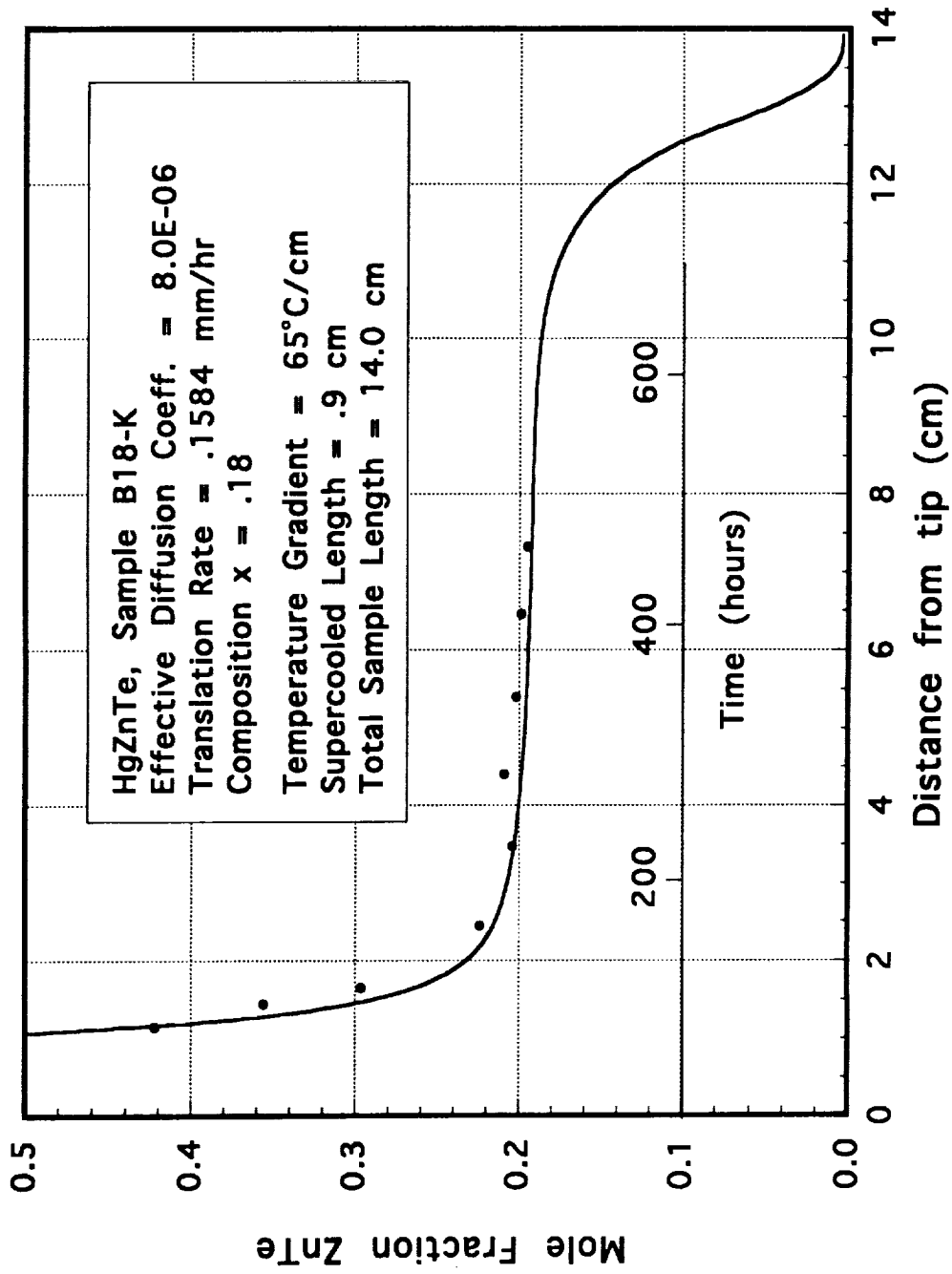
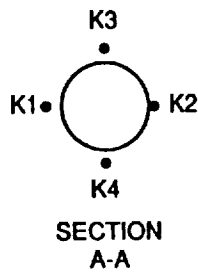
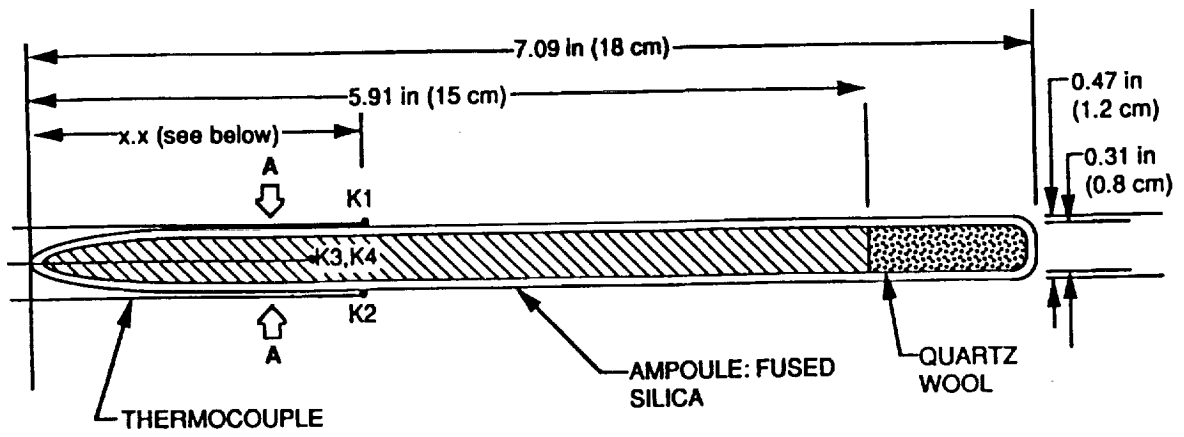
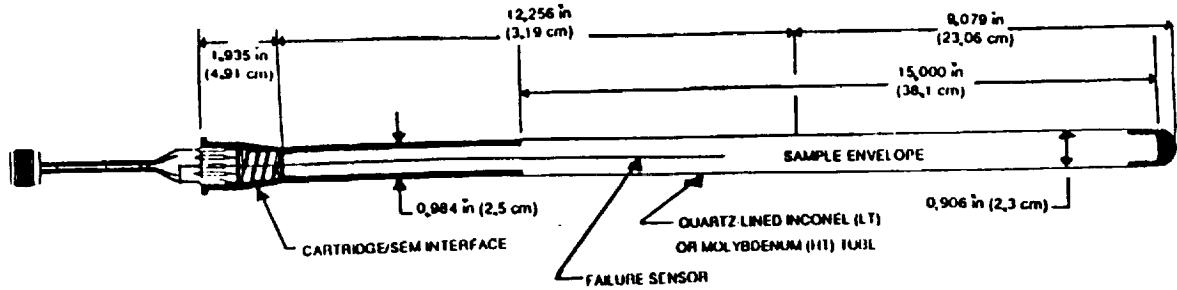


Figure 7 Axial variation in an Hg<sub>0.82</sub>Zn<sub>0.18</sub>Te alloy crystal showing measured and calculated results.



Thermocouple	x.x (Nominal Distance From Ampoule End)
K1	2.36 in (6 cm)
K2	2.36 in (6 cm)
K3	1.97 in (5 cm)
K4	1.97 in (5 cm)

(a)



(b)

Figure 8 Schematic drawing of sample ampoule (a) and cartridge (b) configurations.

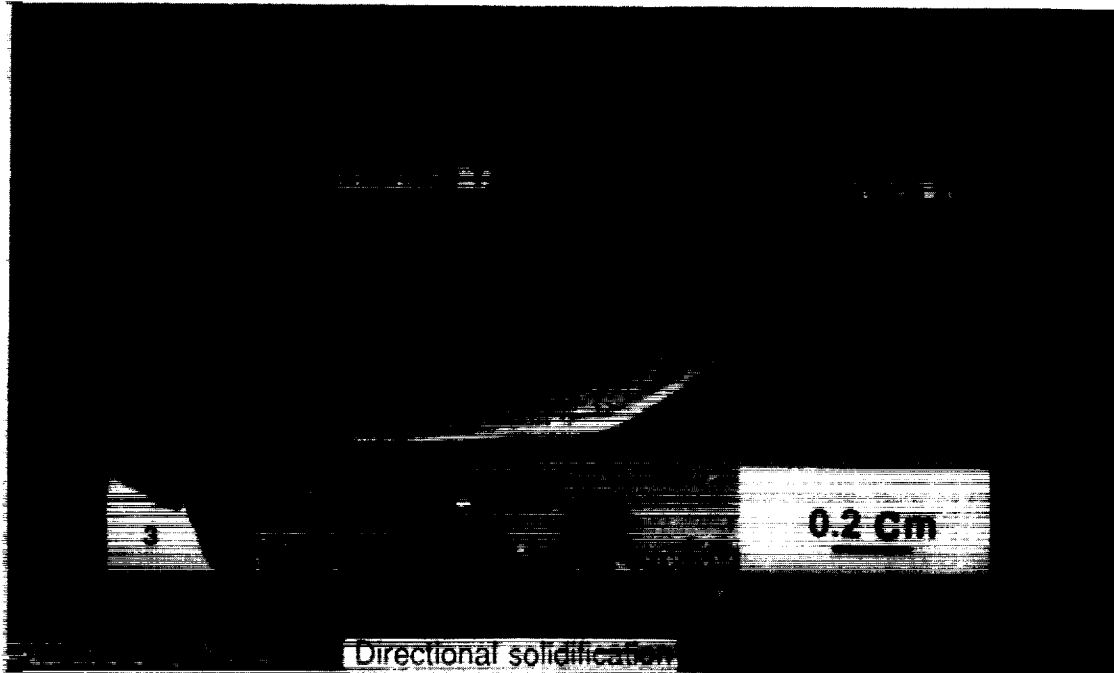


Figure 9 Grain structure near the quenched, back-melted and regrowth interface.

# Zn Content in $\text{Hg}_{1-x}\text{Zn}_x\text{Te}$ B16-1A-B

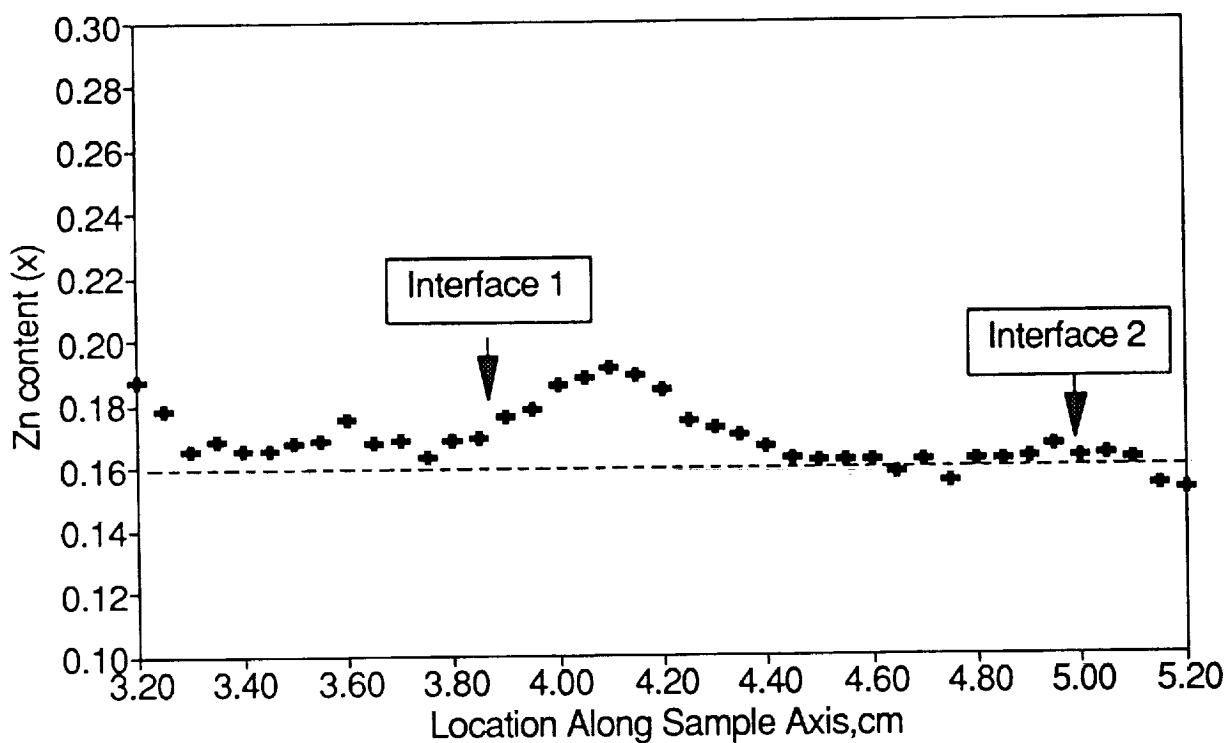


Figure 10 Axial compositional distribution following back-melt/regrowth sequence.

C-3.

4.3 cm

6.5 c

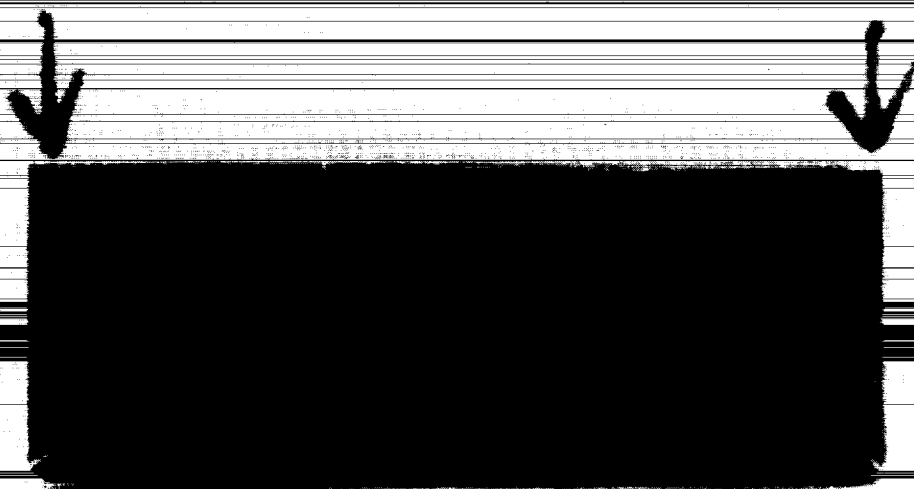


Figure 11 Interface shape for a hot zone temperature of 800°C and a cold zone temperature of 555°C.



Figure 12 Interface shape for a hot zone temperature of 780 °C and a cold zone temperature of 350 °C.

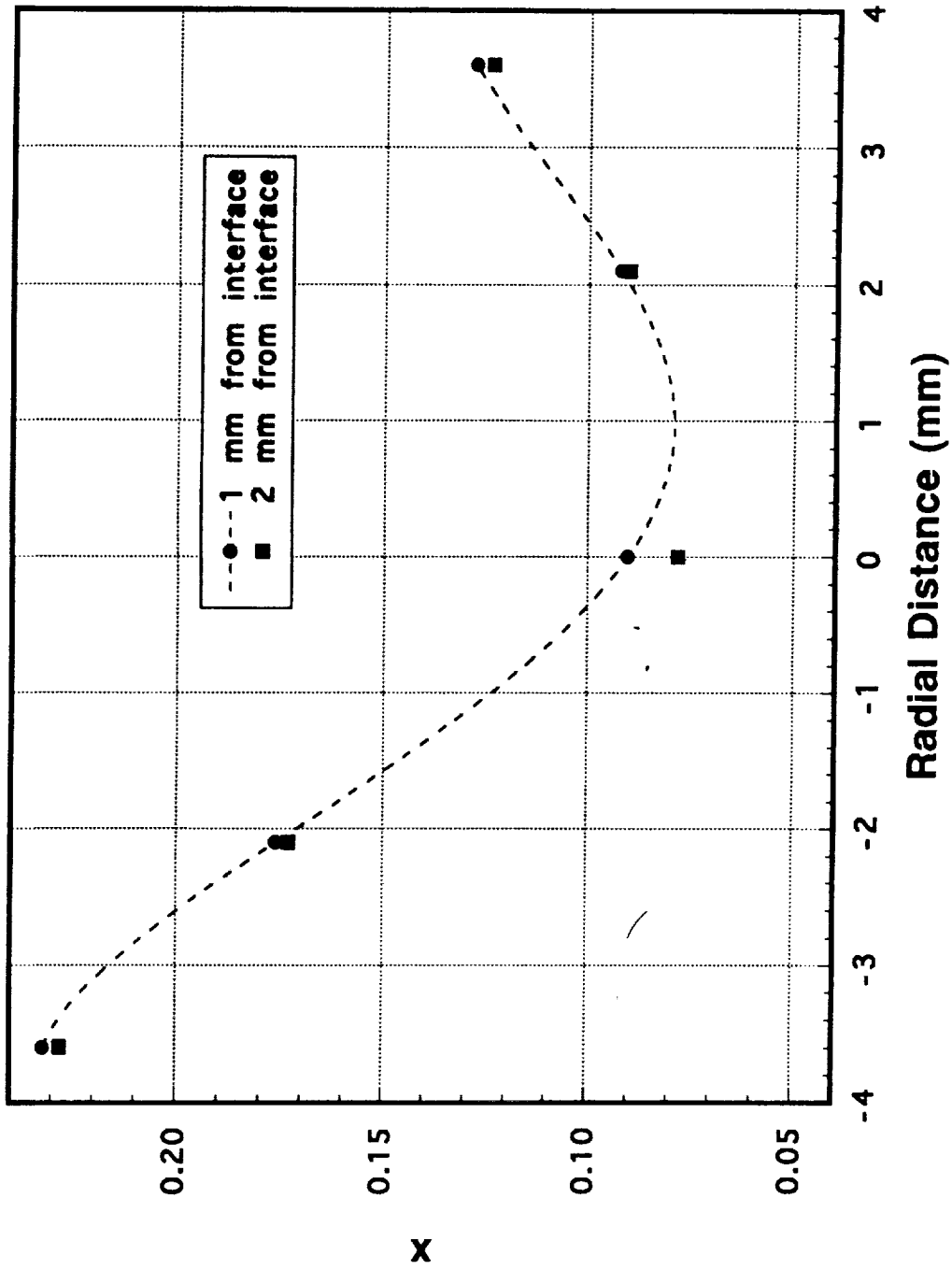


Figure 13 Radial compositional variation for ingot shown in Figure 11.

# Radial Distribution

Sample: B16-2

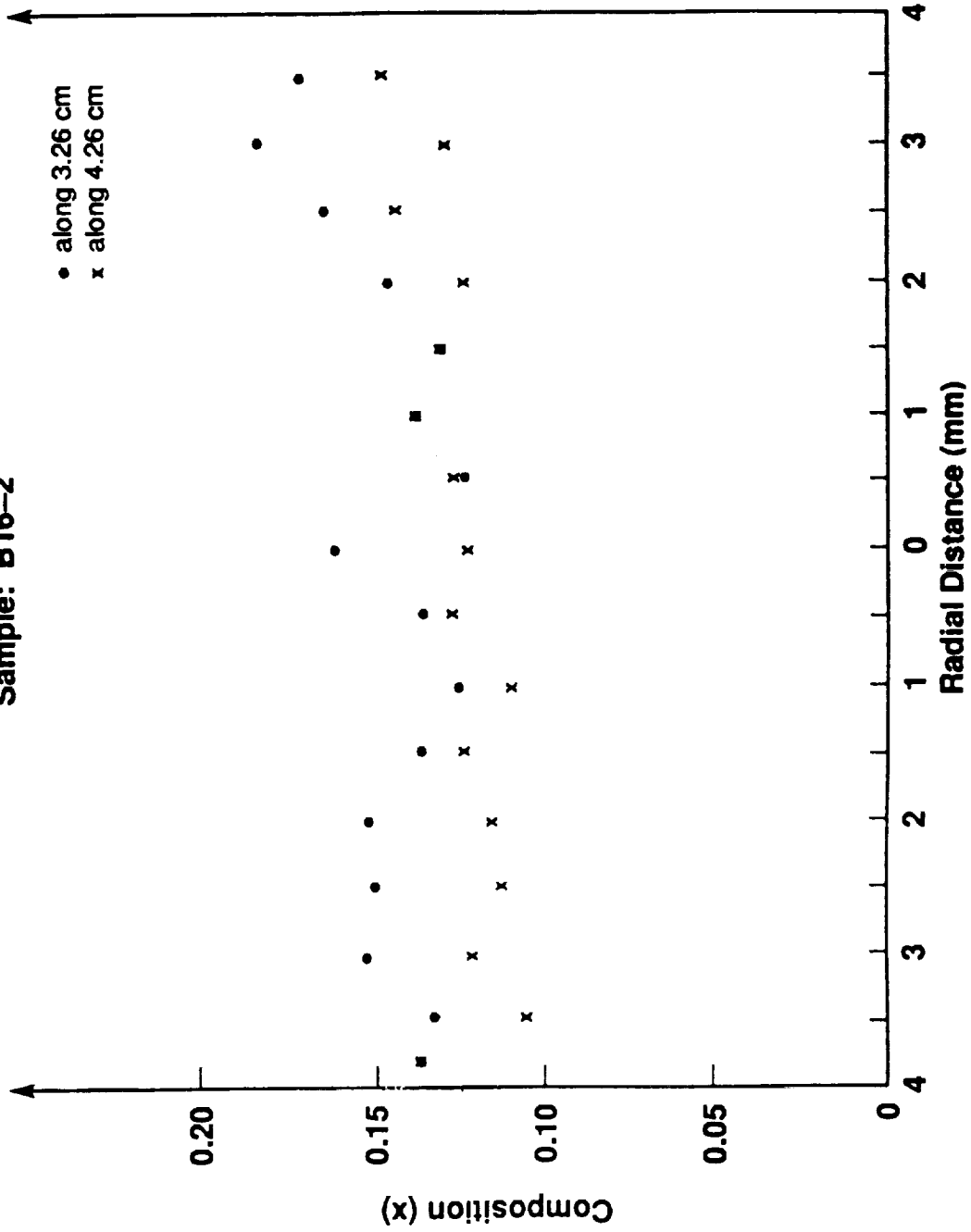


Figure 14 Radial compositional variation for ingot shown in Figure 12. The data were measured along 3.26 and 4.26 cm from the first freeze (the interface is at about 5.3 cm from the first freeze).

inadvertent  
experiment  
termination

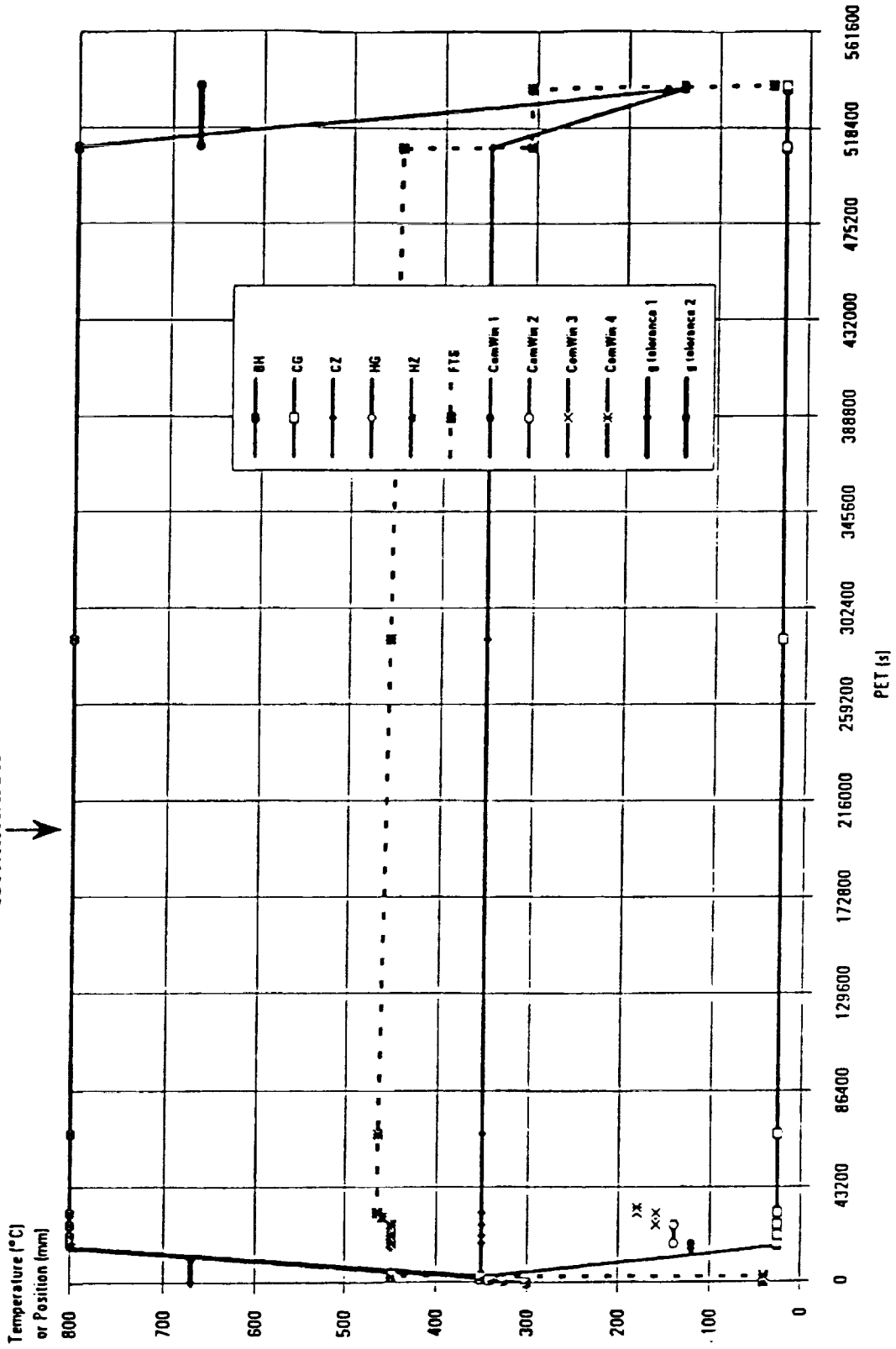


Figure 15 Scheduled USML-1 timeline.



**MSFC JULY 1492**

**S/N08 B16-7**



**270**

**180**

**90**

**0**

Figure 16 Radiograph of returned flight sample.

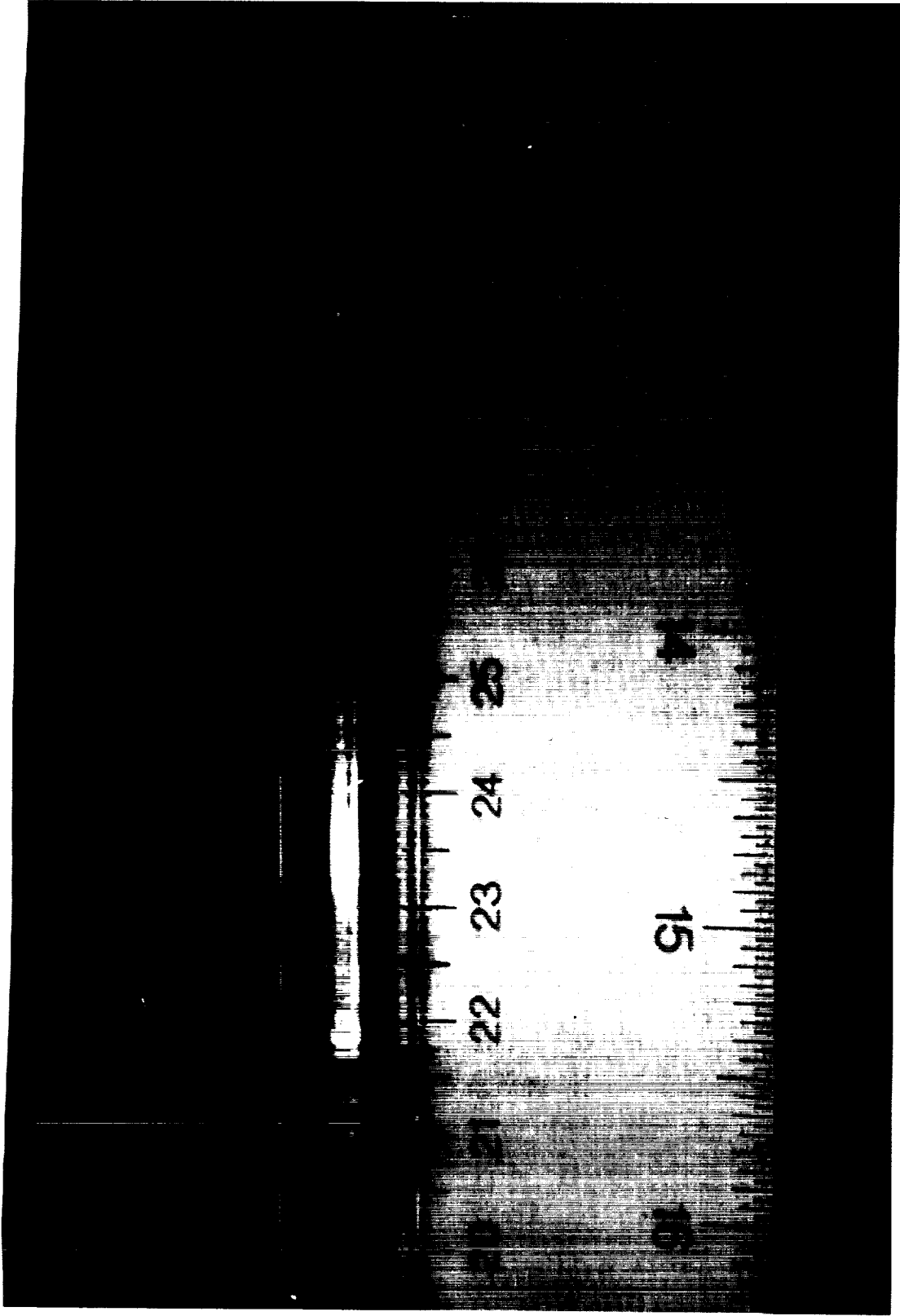


Figure 17 Flight sample photograph inside fused-silica ampoule.



Figure 18 Surface photomicrograph of space grown region.

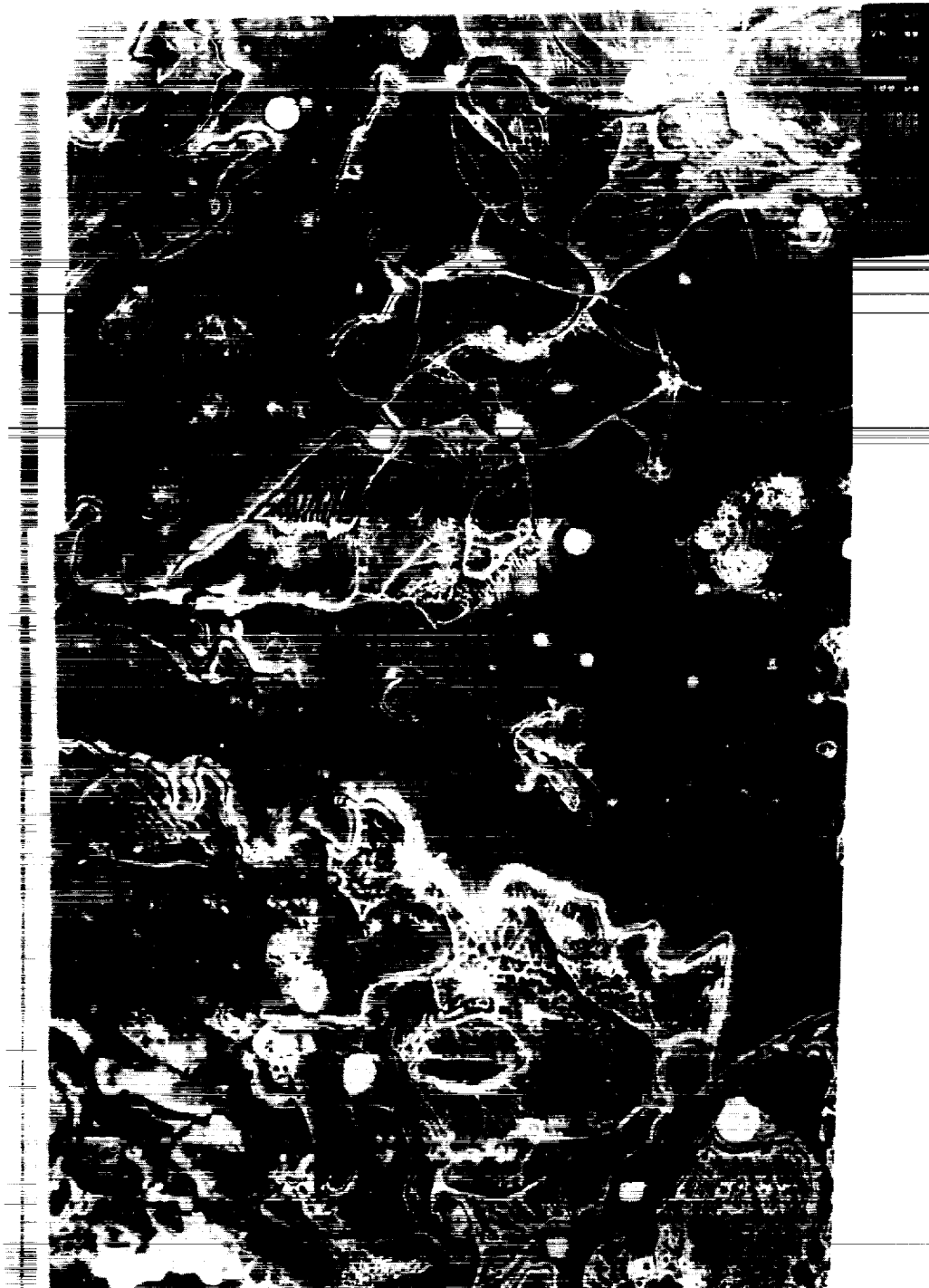


Figure 19 Surface photomicrograph of ground-truth sample for same axial location as for flight sample shown in Figure 18.

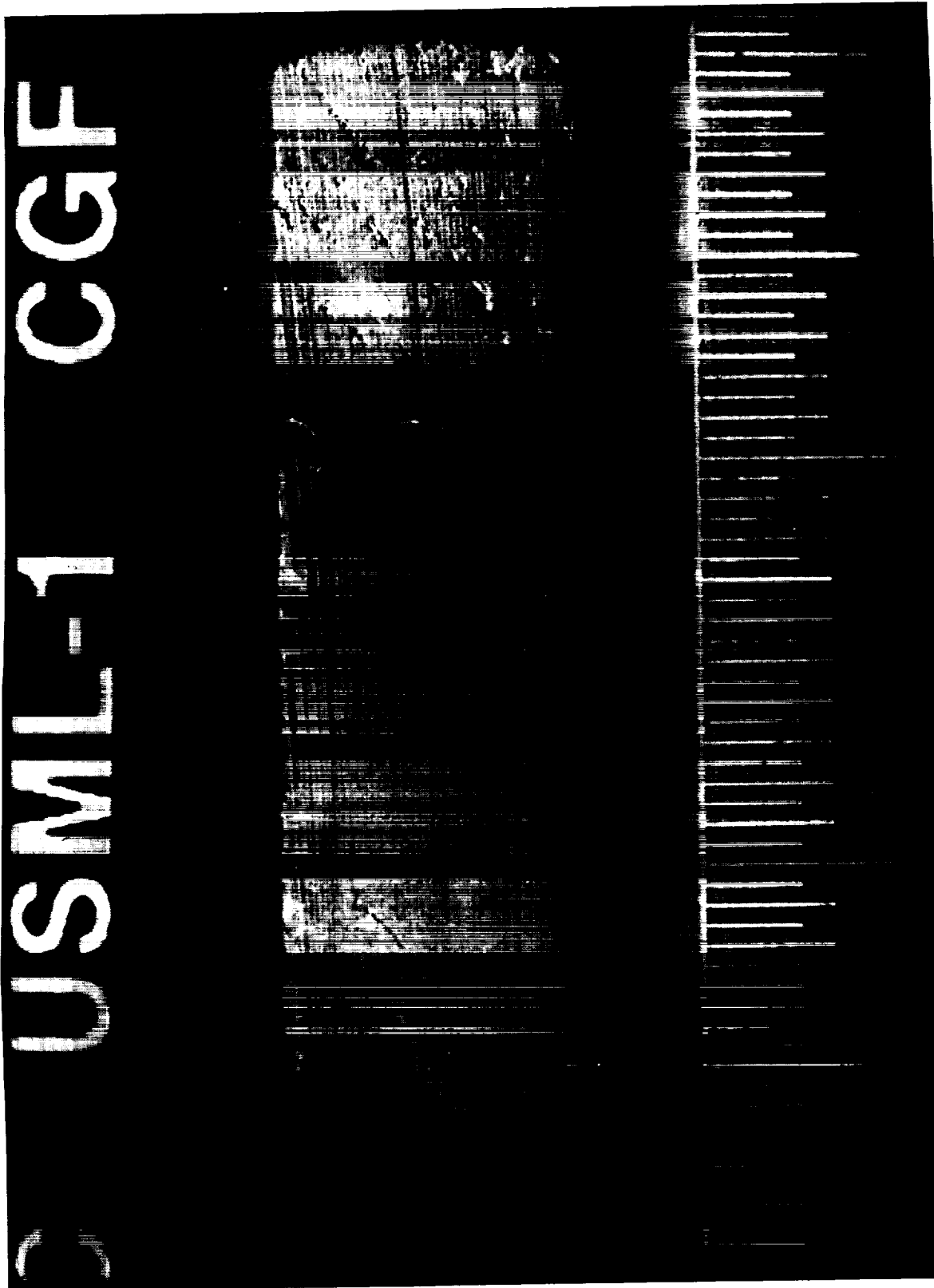


Figure 20 Quenched-in melt/solid interface shown in a longitudinal section cut from the flight sample.

# HgZnTe Ground Truth Sample

## 4.7 --- 6.3 cm from FTF



Figure 21 Quenched-in melt/solid interface shown in a longitudinal section cut from "ground-truth" sample after annealing. (Note that the cut is not exactly perpendicular to the crystal axis.)



Figure 22 Photomicrograph of polished and bromine-etched slab from flight sample.

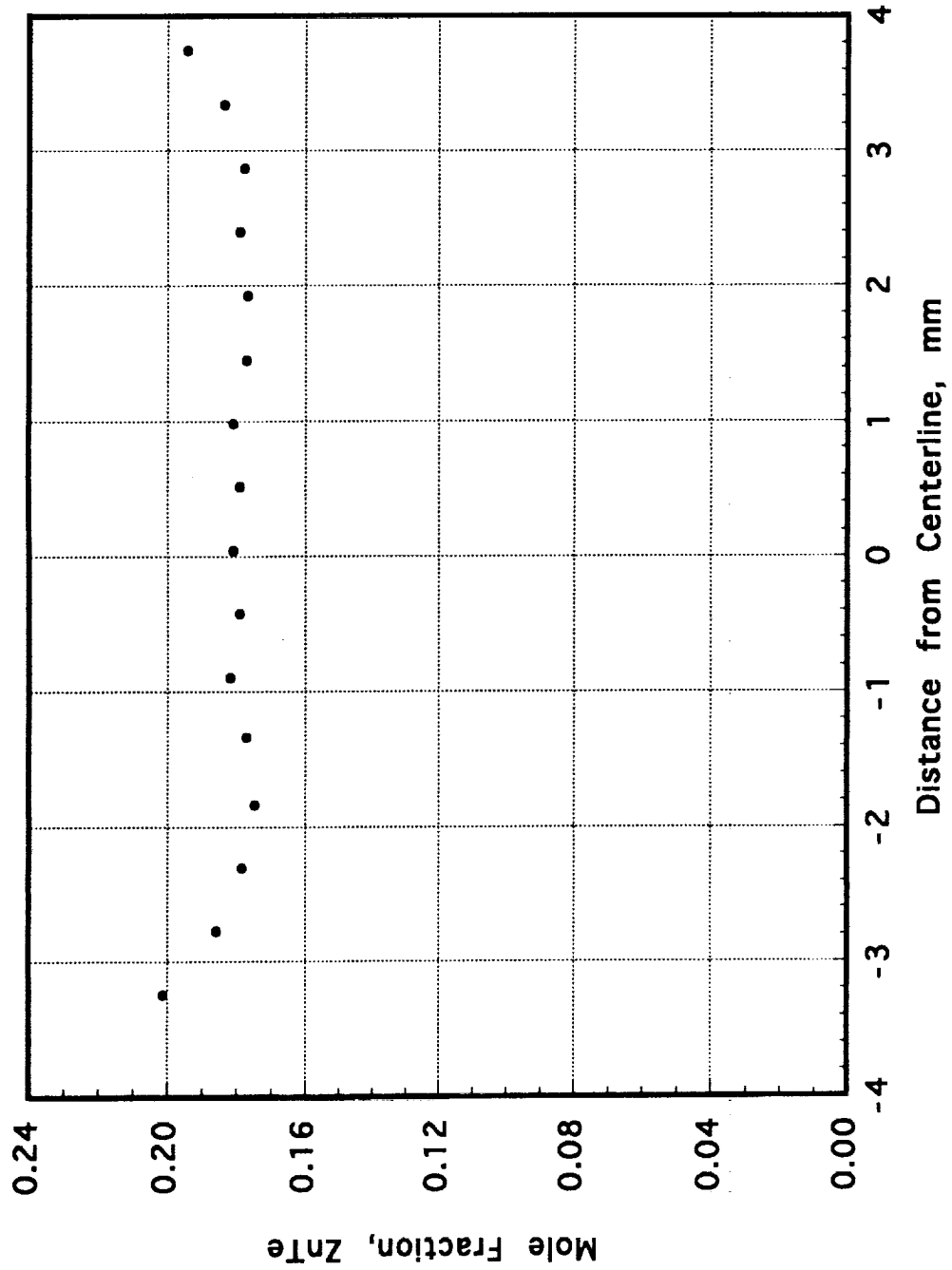


Figure 23 Flight sample radial compositional distribution 6 mm from quenched-in interface.

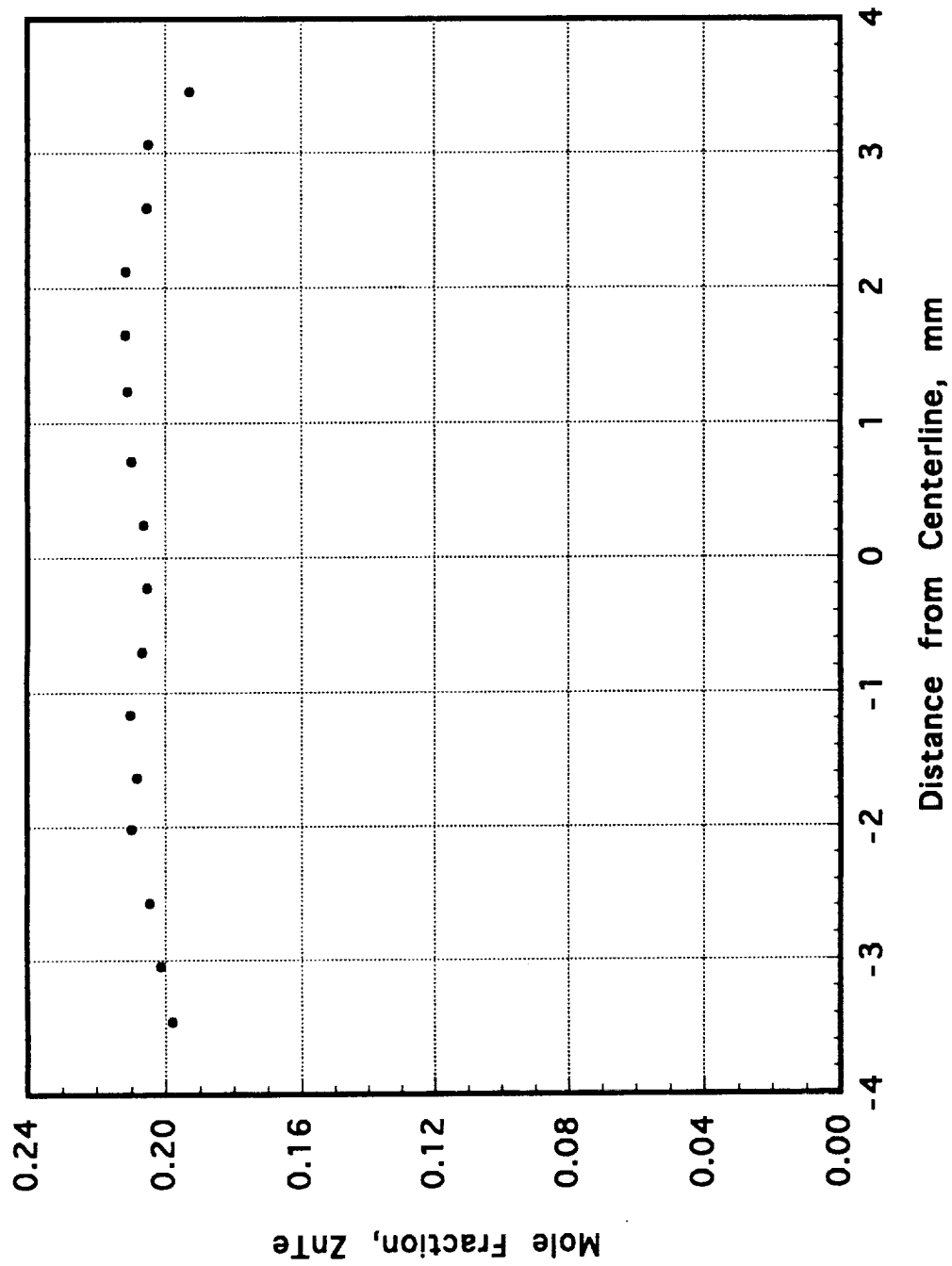


Figure 24 Flight sample radial compositional distribution 5 mm from quenched-in interface.

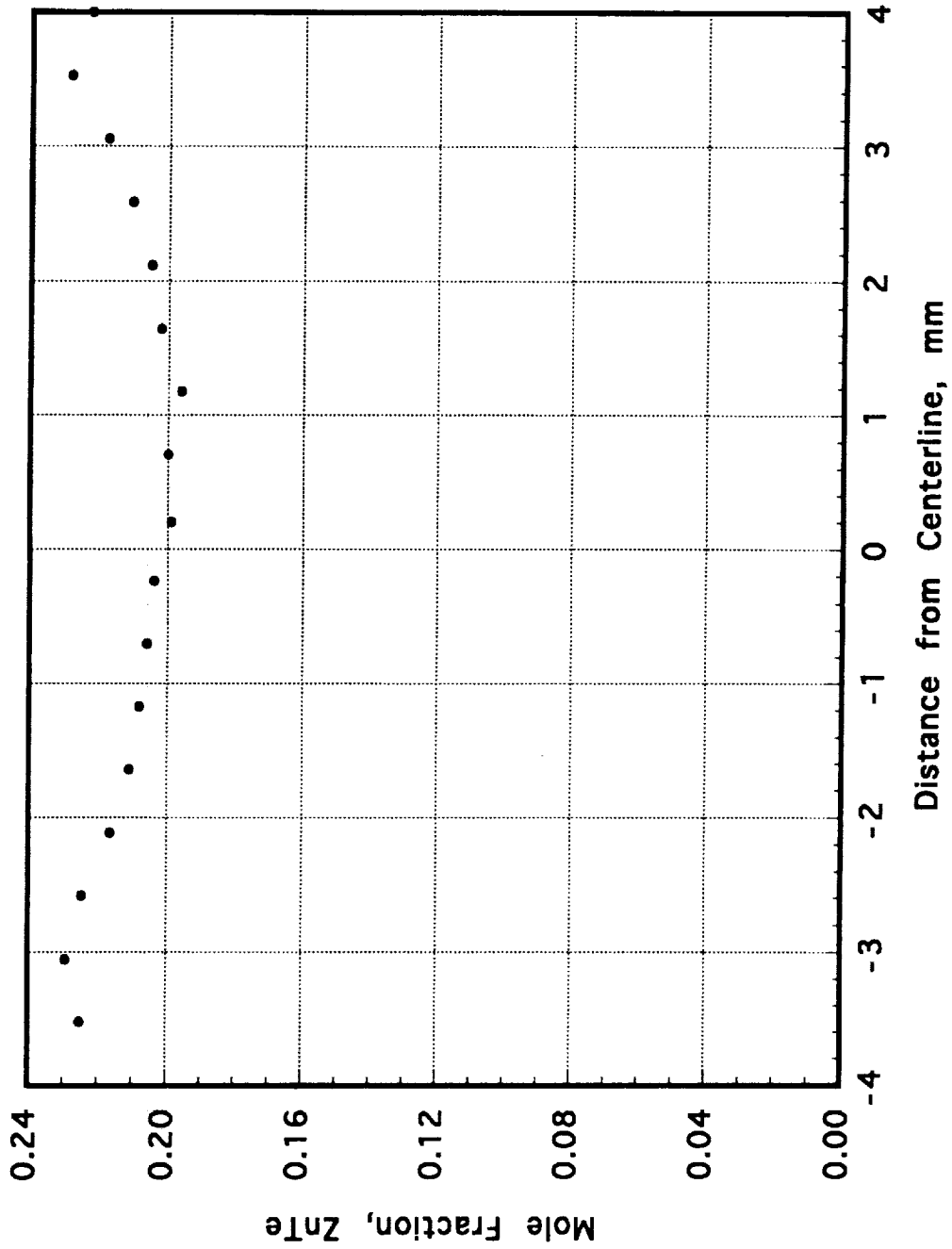


Figure 25 Flight sample radial compositional distribution 4 mm from quenched-in interface.

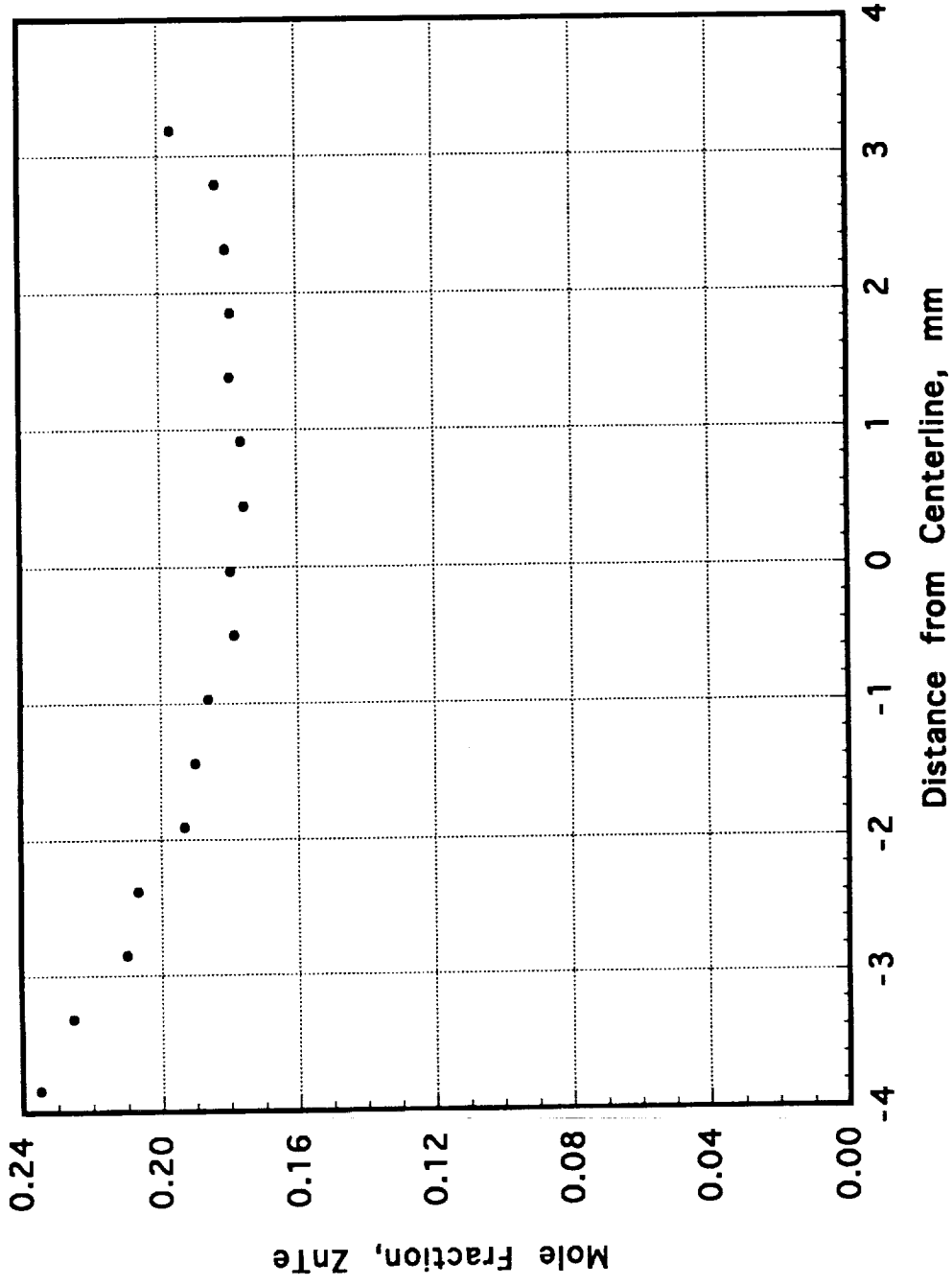


Figure 26 Flight sample radial compositional distribution 3 mm from quenched-in interface.

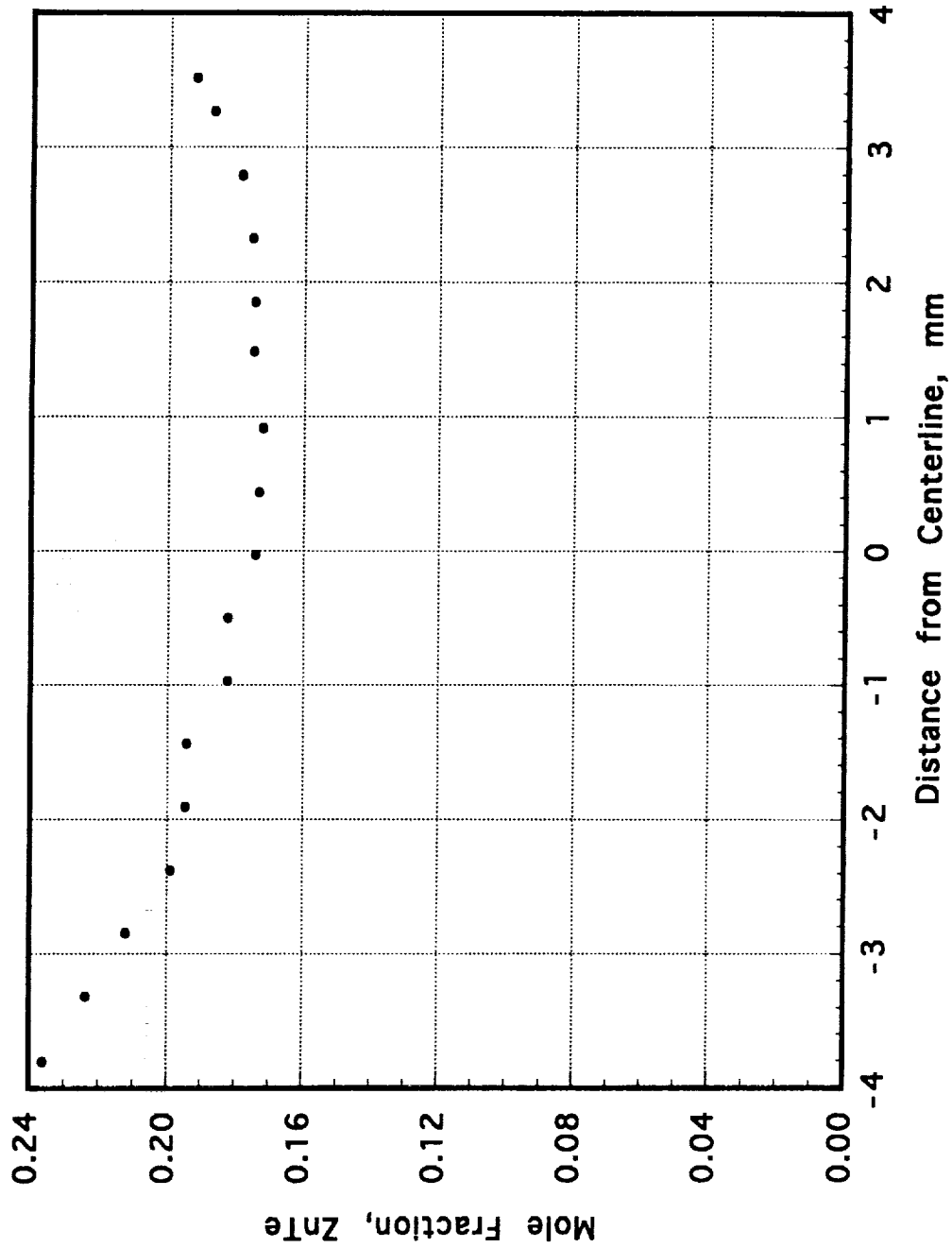


Figure 27 Flight sample radial compositional distribution 2 mm from quenched-in interface.

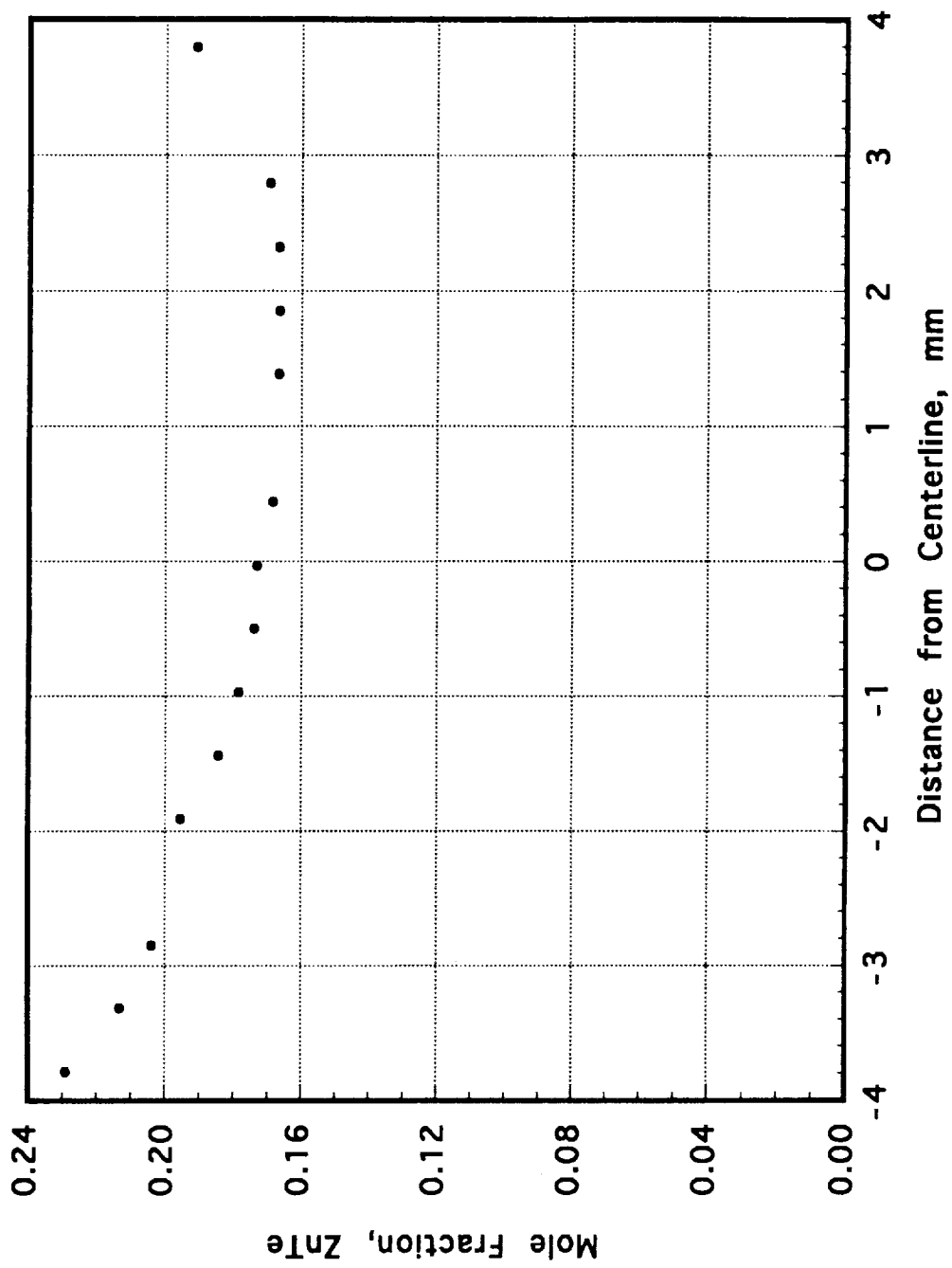


Figure 28 Flight sample radial compositional distribution 1 mm from quenched-in interface.

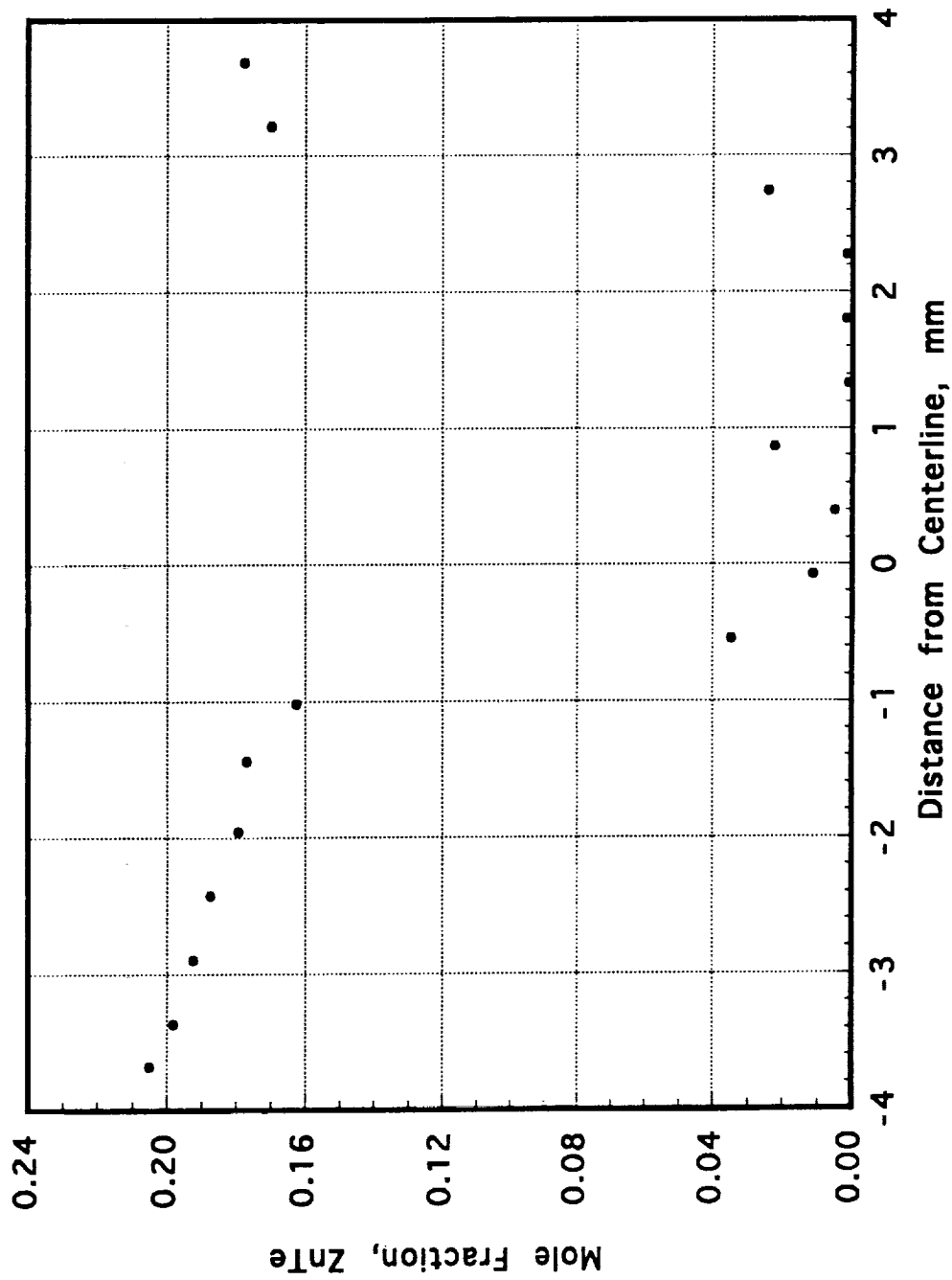


Figure 29 Flight sample radial compositional distribution at the interface.

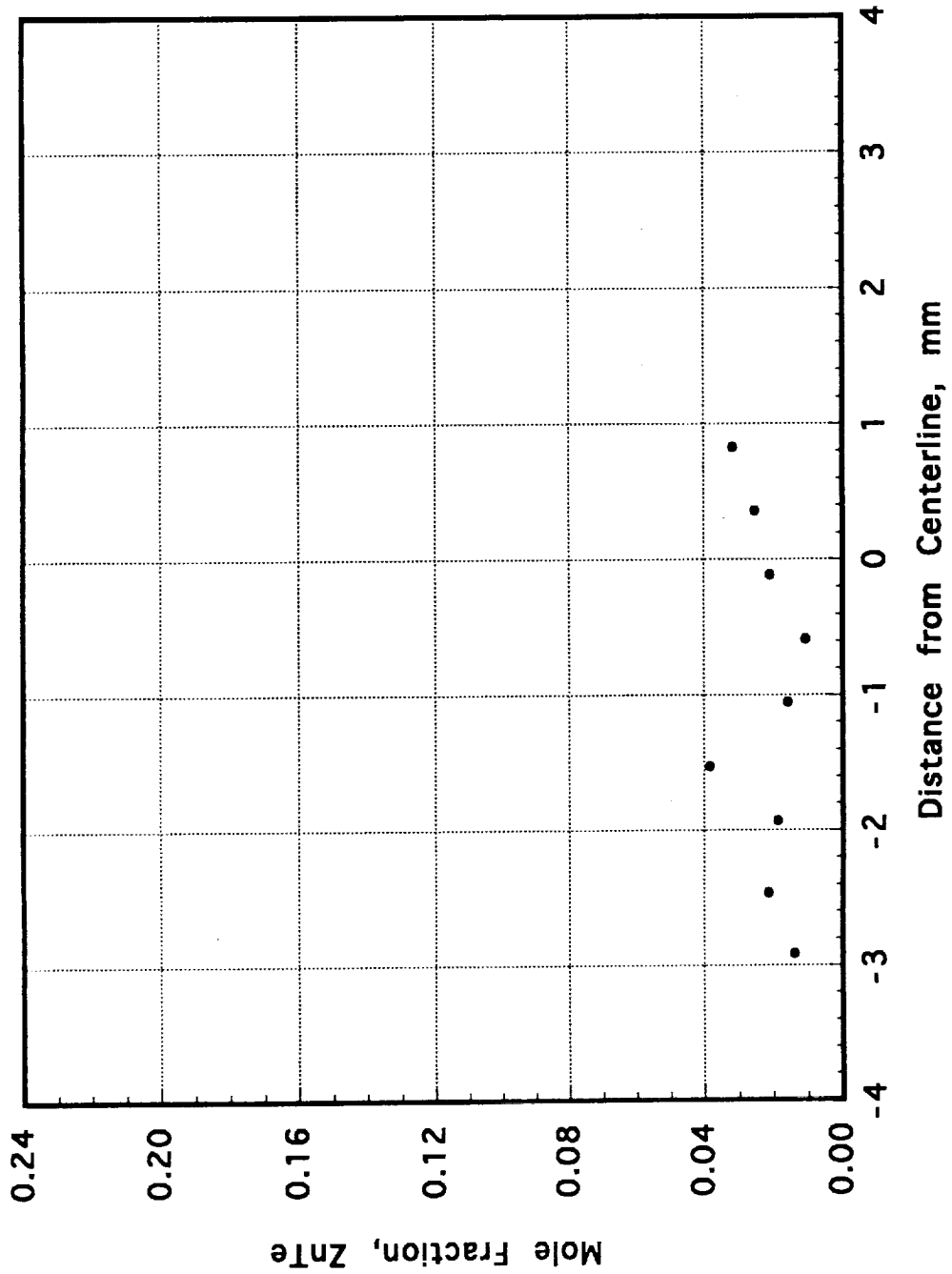


Figure 30 Flight sample radial compositional distribution 1 mm past interface.

— AX, ug

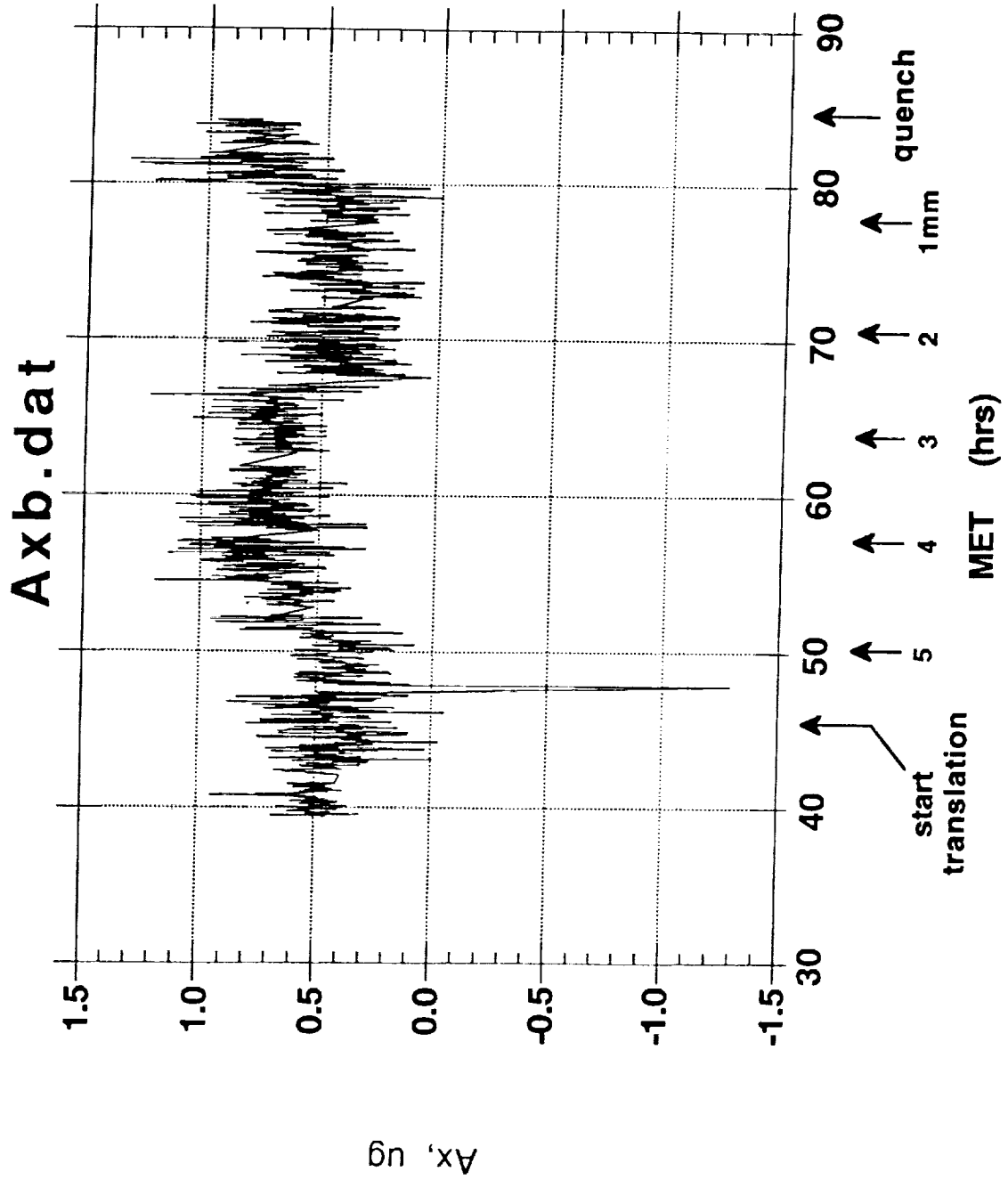
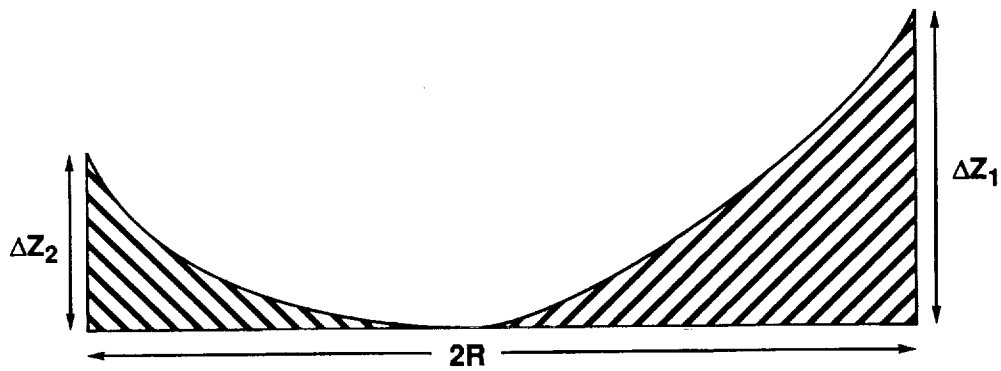


Figure 31 OARE acceleration data for the growth duration.

## Interface Deflection and Radial Segregation



$$\frac{\delta C}{C_0} = \frac{(k-1)}{k} \frac{R}{D} \Delta Z$$

**k = Segregation Coefficient = 4.0**

**D = Effective ZnTe - HgTe Liquid Diffusion Coefficient  
=  $6 \times 10^{-6} \text{ cm}^2/\text{s}$**

**R = Growth Rate =  $4.0 \times 10^{-6} \text{ cm/s}$**

Figure 32 Correlation between interface deflection and relative radial segregation.

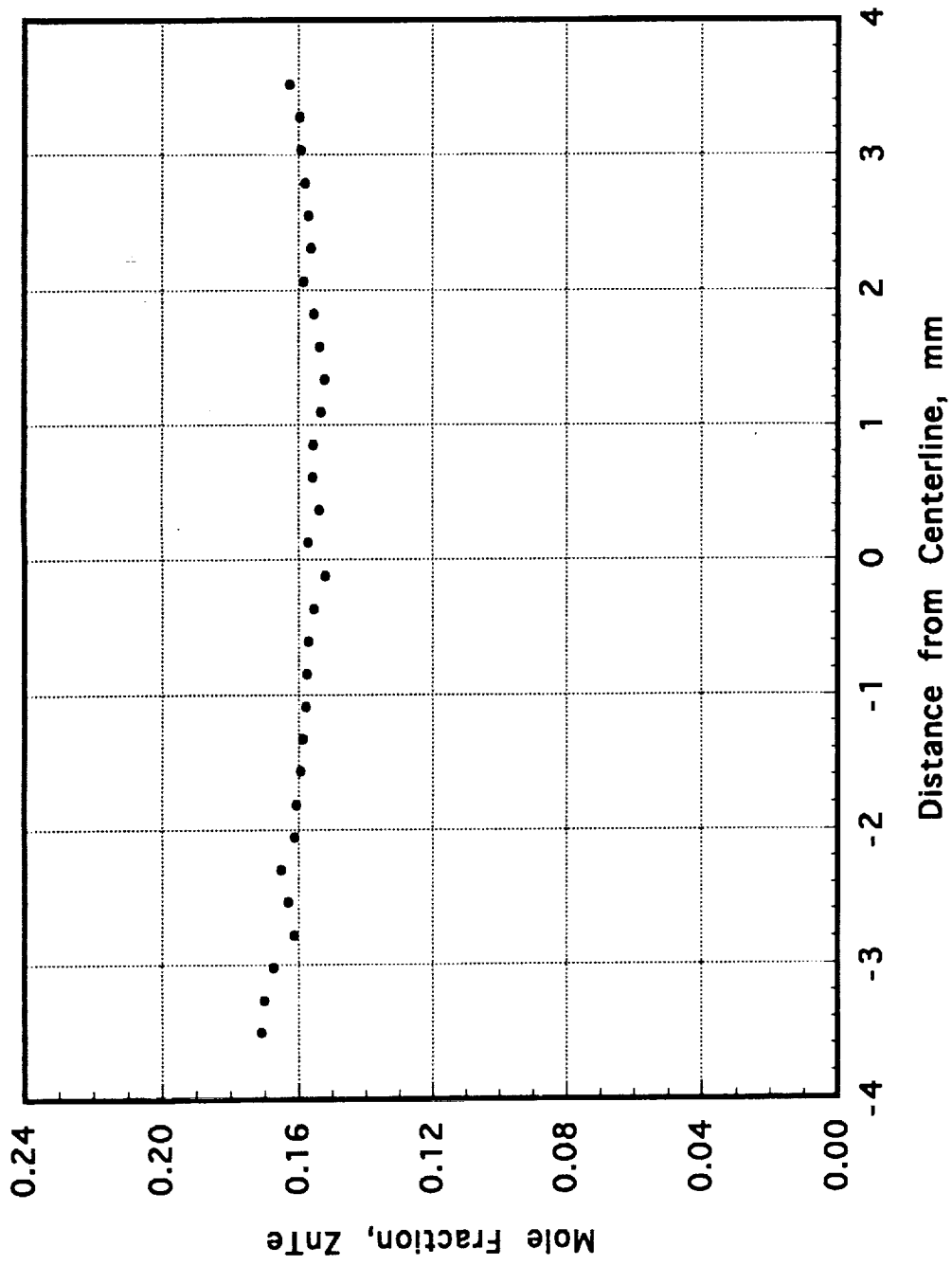


Figure 33 Ground-truth sample radial composition 6 mm from quenched-in interface.

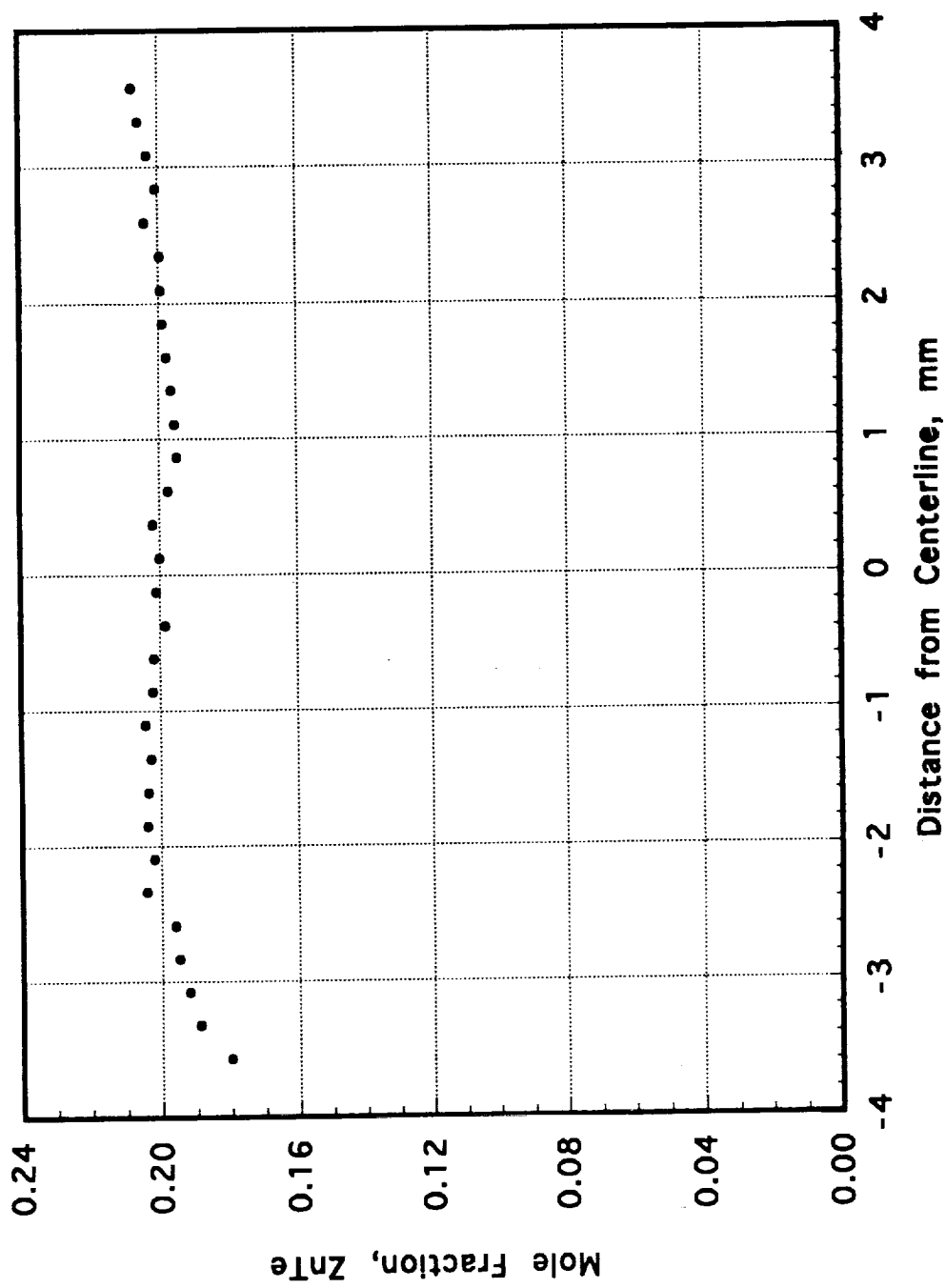


Figure 34 Ground-truth sample radial composition 4 mm from quenched-in interface.

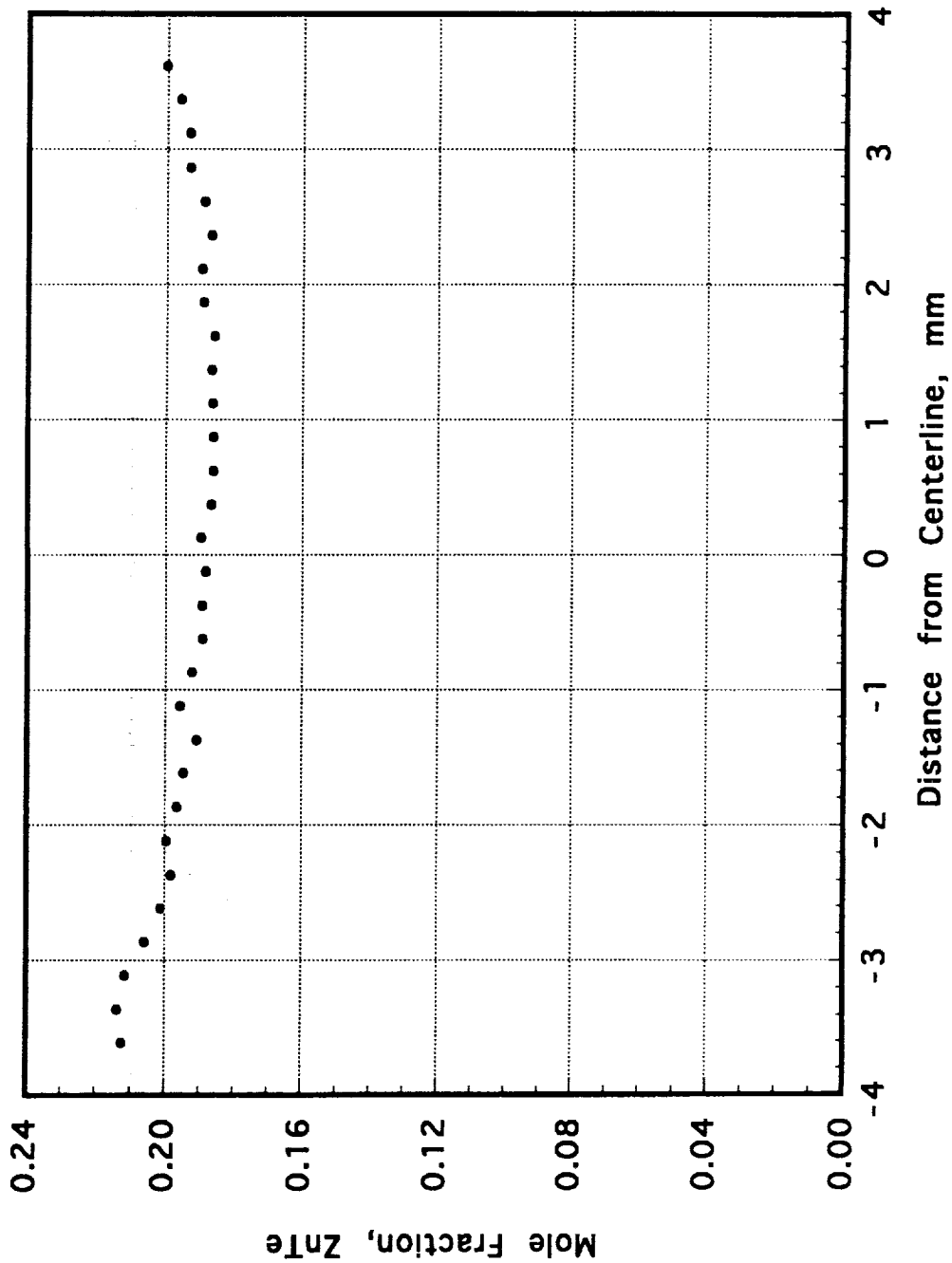


Figure 35 Ground-truth sample radial composition 3 mm from quenched-in interface.

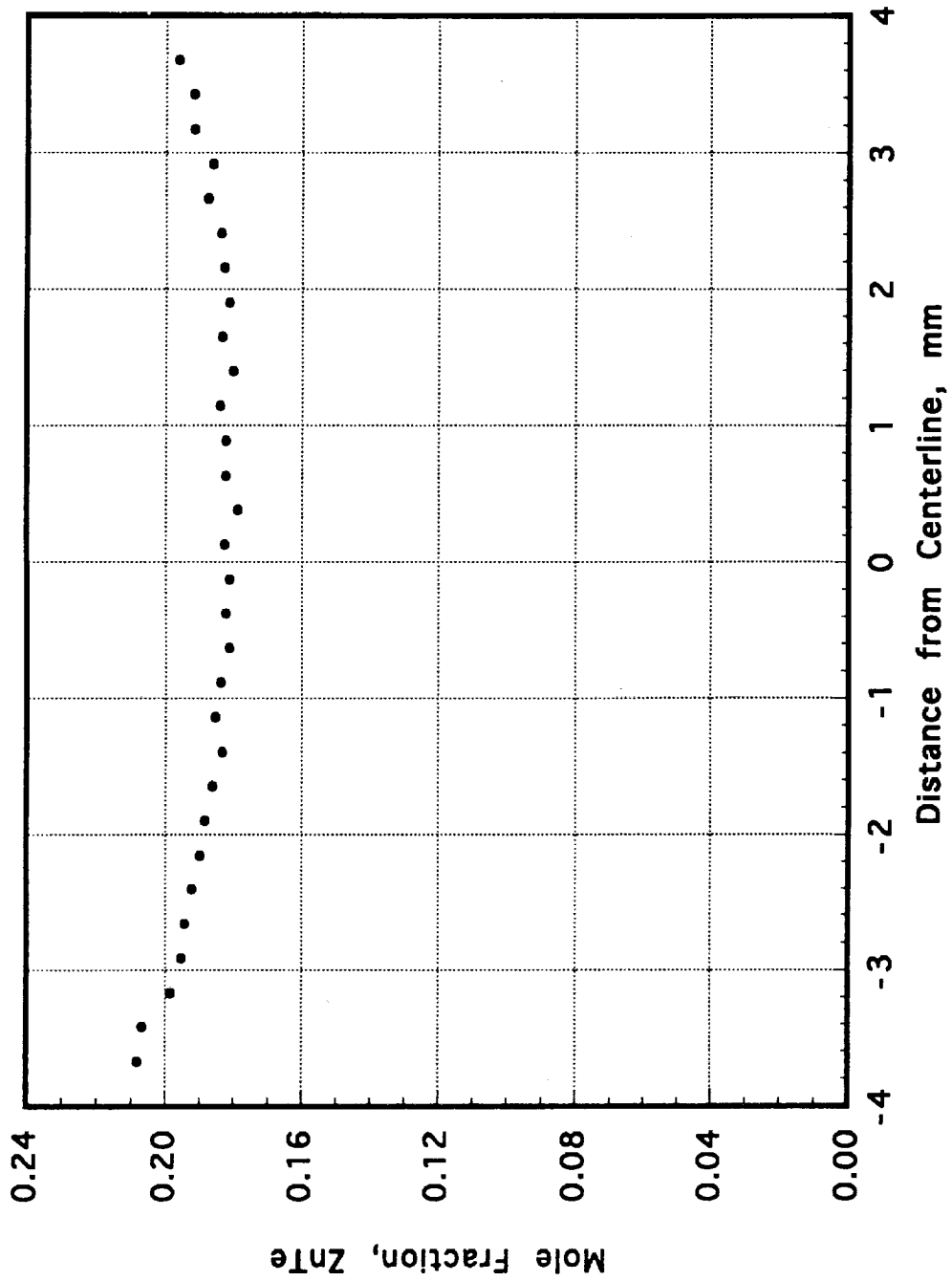


Figure 36 Ground-truth sample radial composition 2 mm from quenched-in interface.

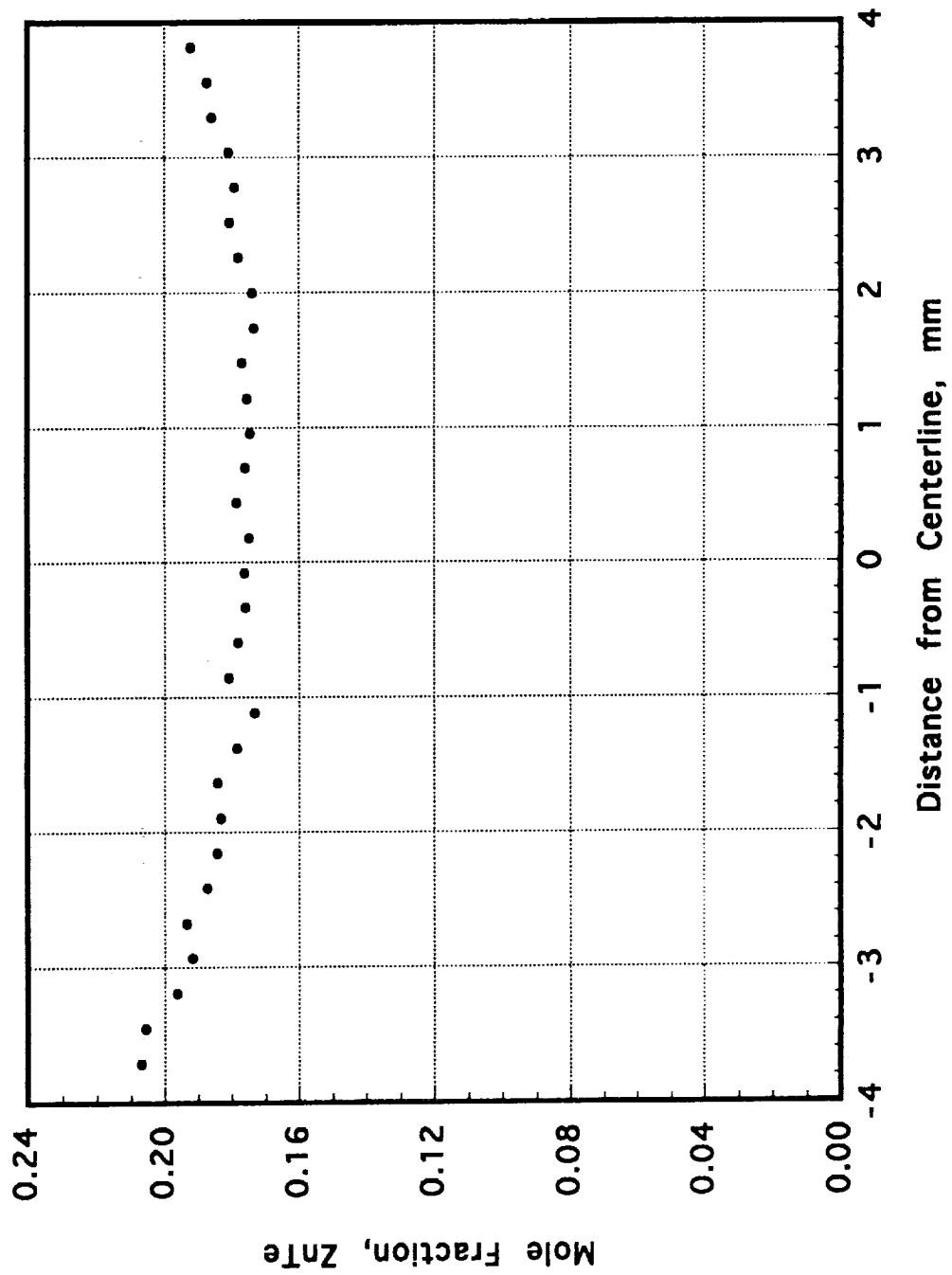


Figure 37 Ground-truth sample radial composition 1 mm from quenched-in interface.

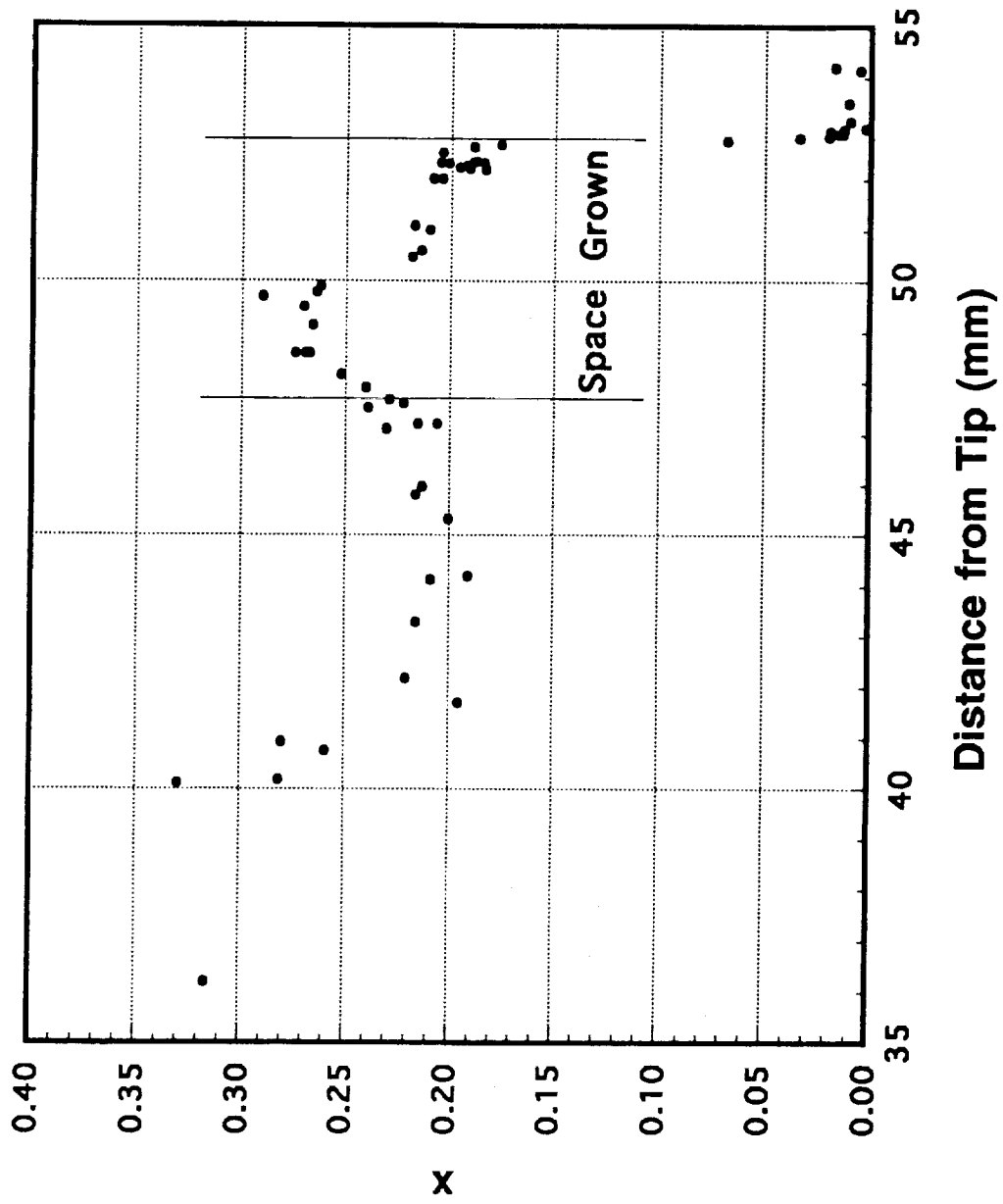


Figure 38 Surface composition distribution along flight sample axis.

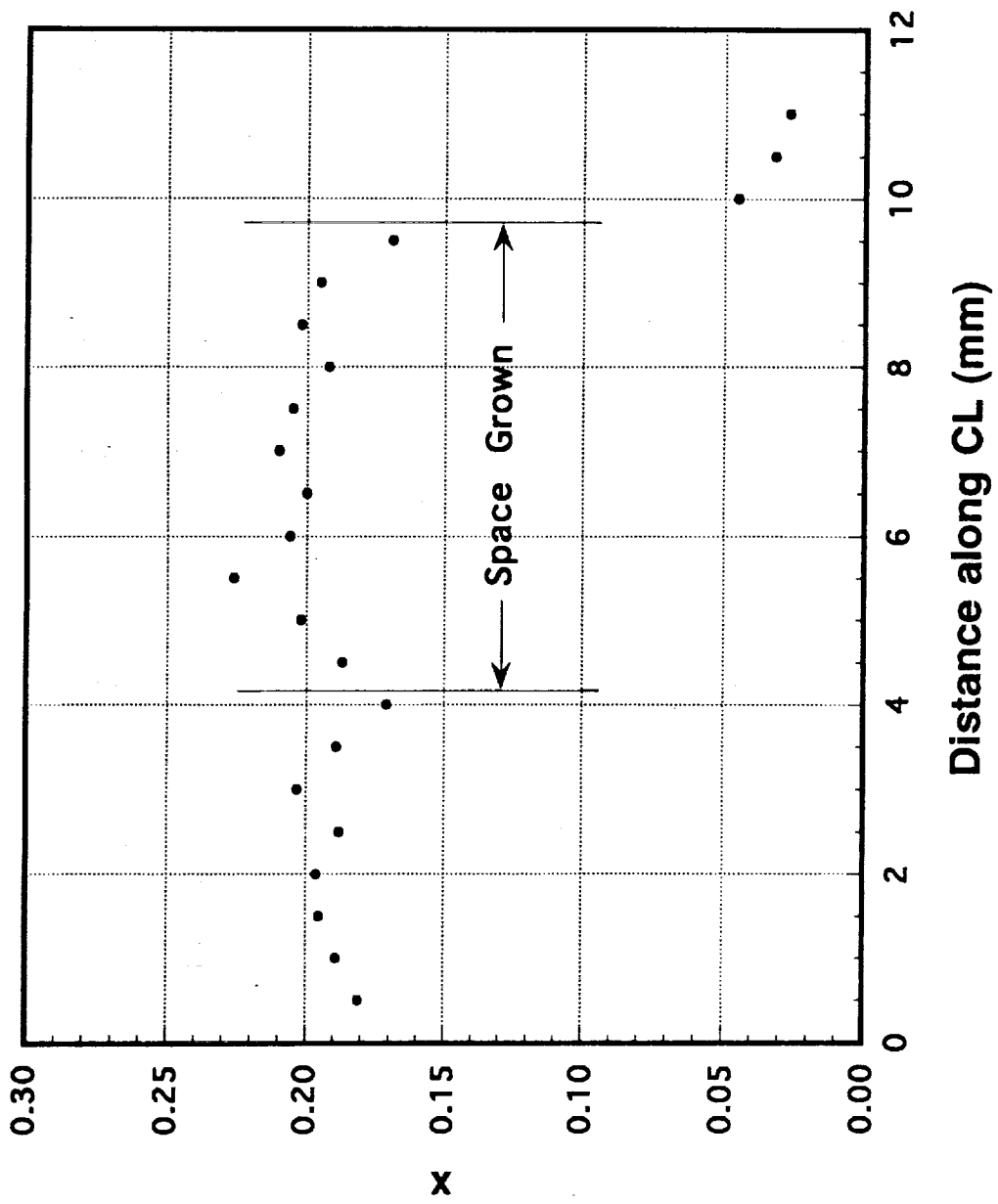


Figure 39 Center-line compositional distribution along flight sample axis.

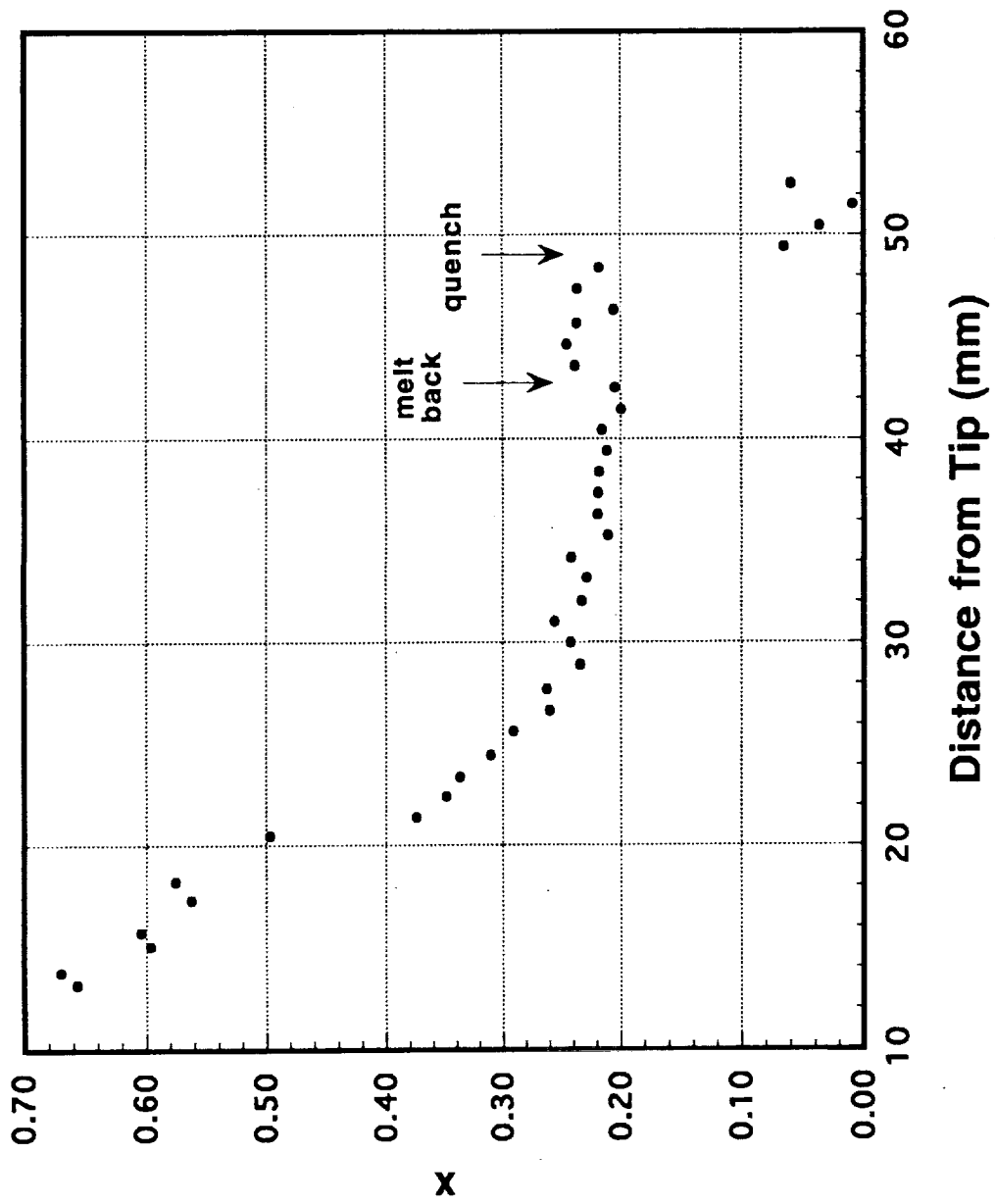


Figure 40 Surface compositional distribution along ground-truth sample axis.

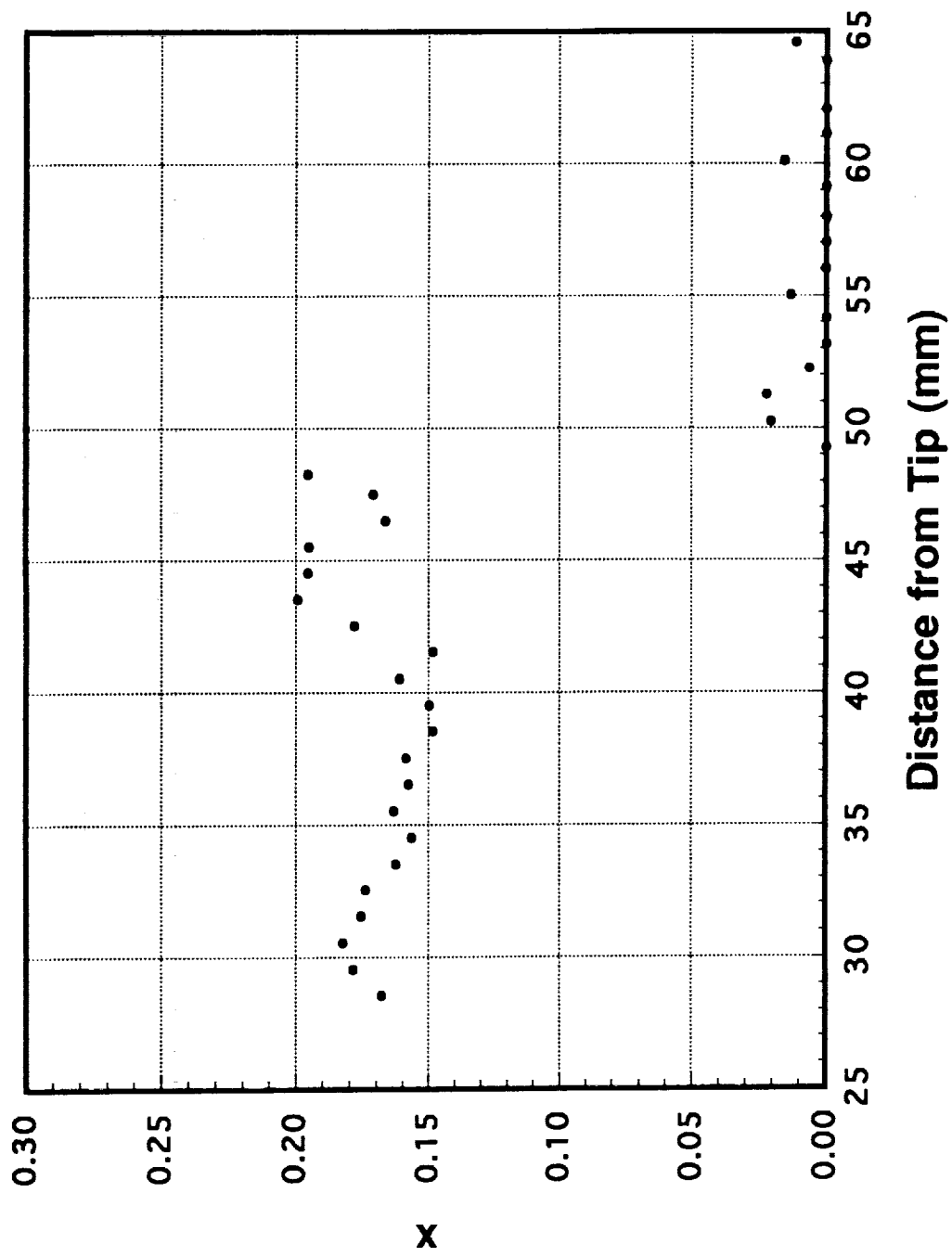


Figure 41 Center-line compositional distribution along ground-truth sample axis.

USML-1 QUENCHED MATERIAL HgZnTe  
Near Interface

500  $\mu\text{m}$

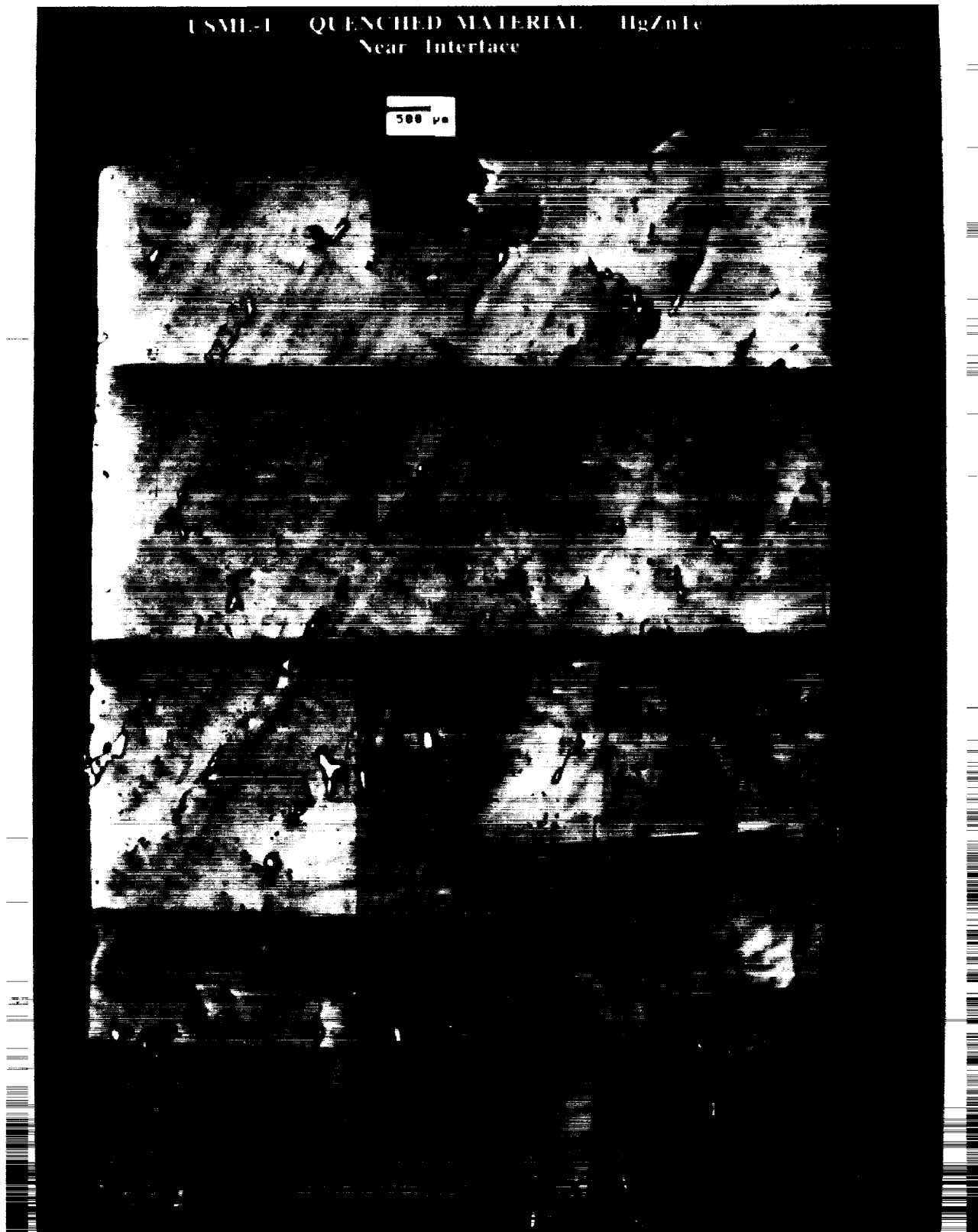


Figure 42 Back scattering SEM micrograph of part of the quenched in portion of flight sample.

B16-34 Ground Truth Sample Quenched HgZnTe  
Near Interface



Figure 43 Back scattering SEM micrograph of part of the quenched in portion of the ground truth sample.

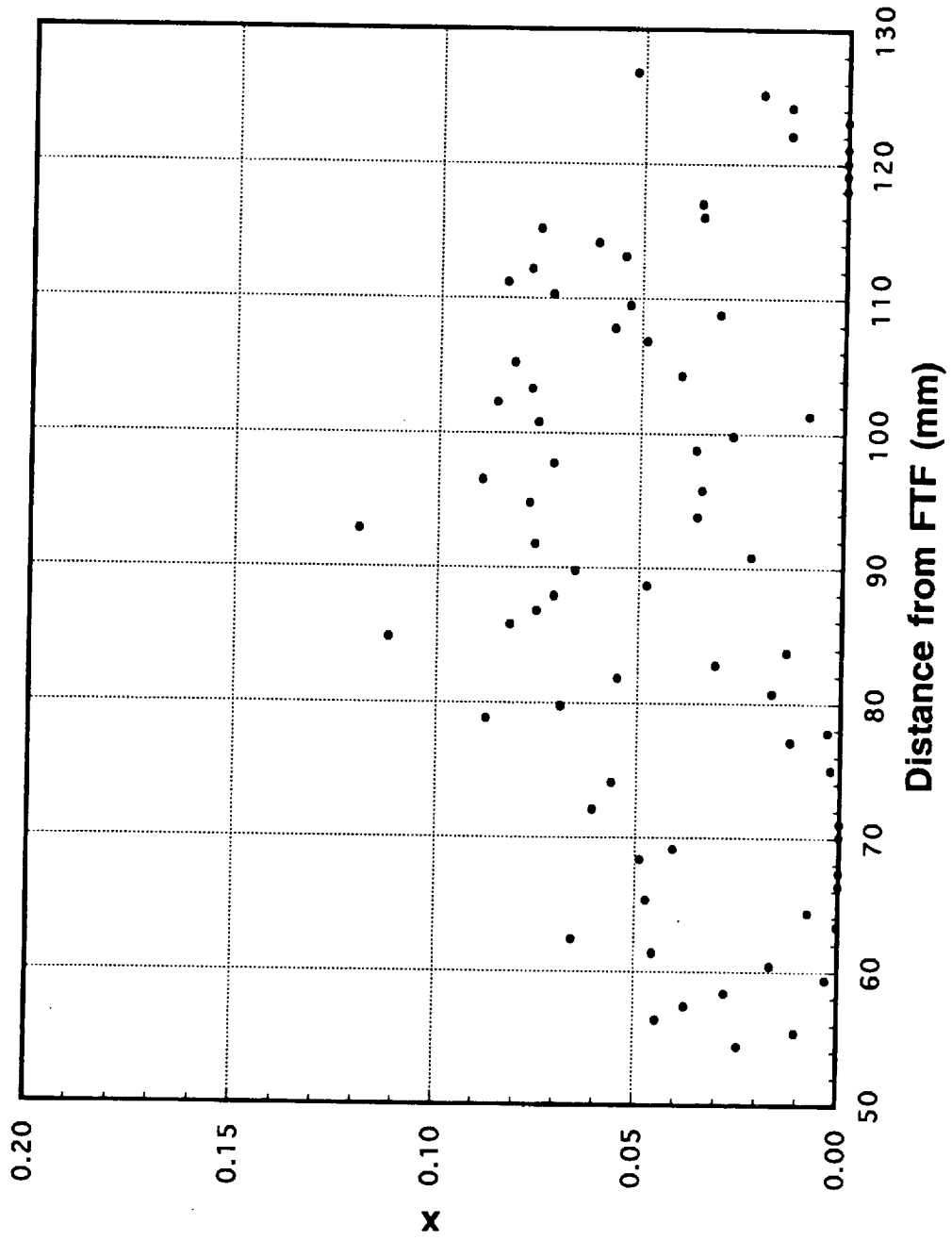


Figure 44 As-grown center-line compositional distribution along a quenched-in portion of the flight sample.

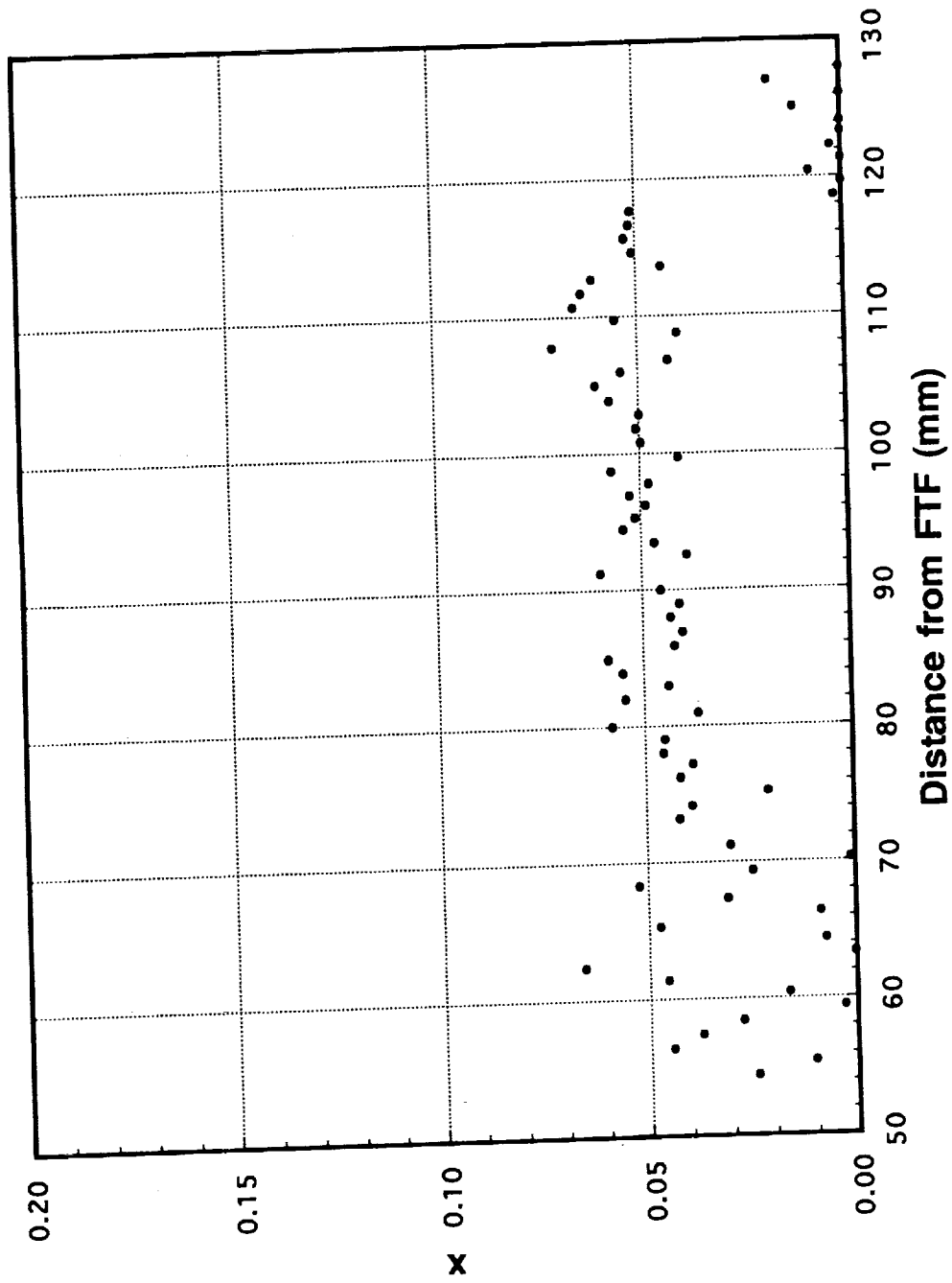


Figure 45 After-anneal center-line compositional distribution along a quenched-in portion of the flight sample.

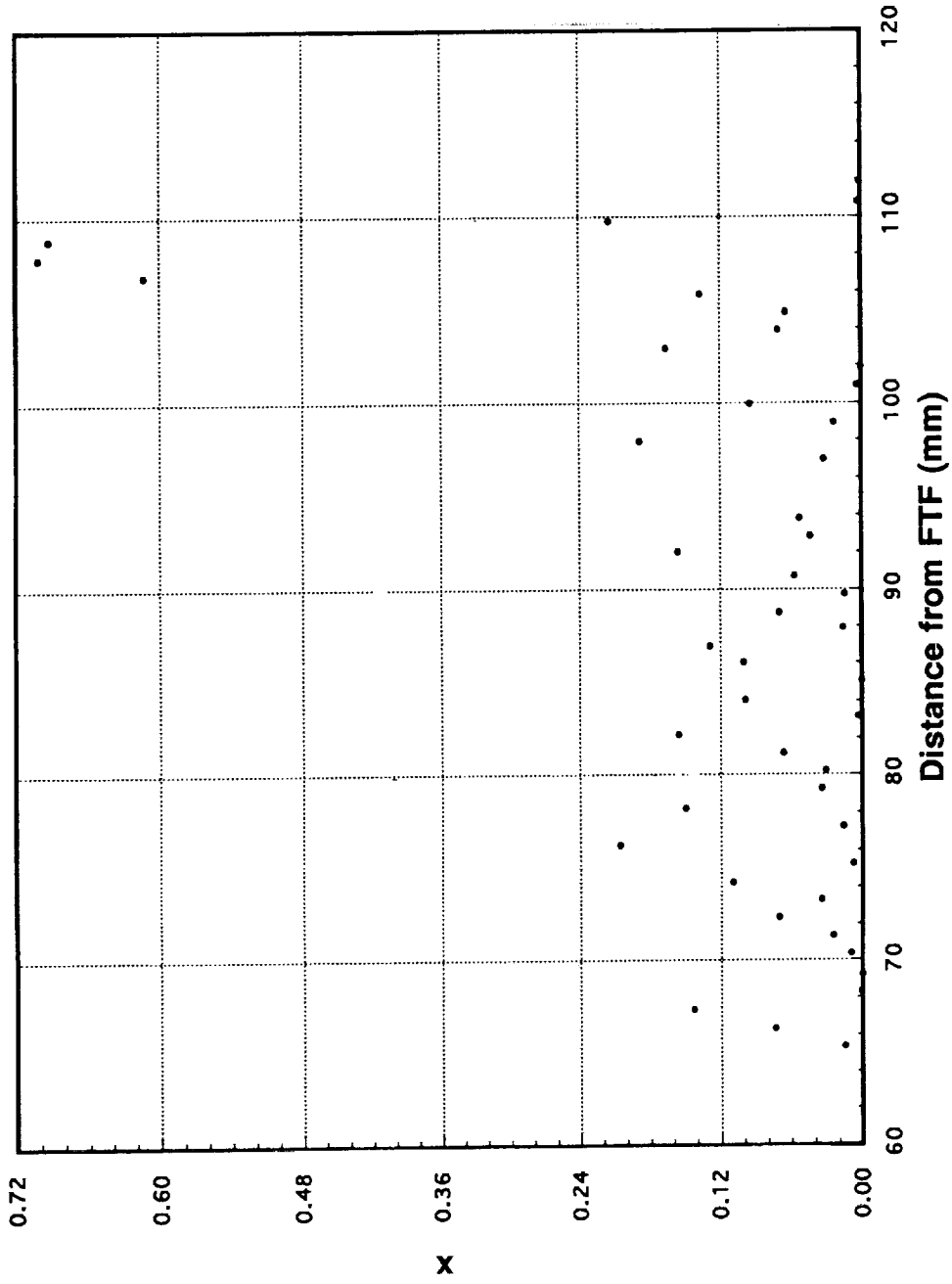


Figure 46 As-grown off-center-line compositional distribution along a quenched-in portion of the ground truth sample.

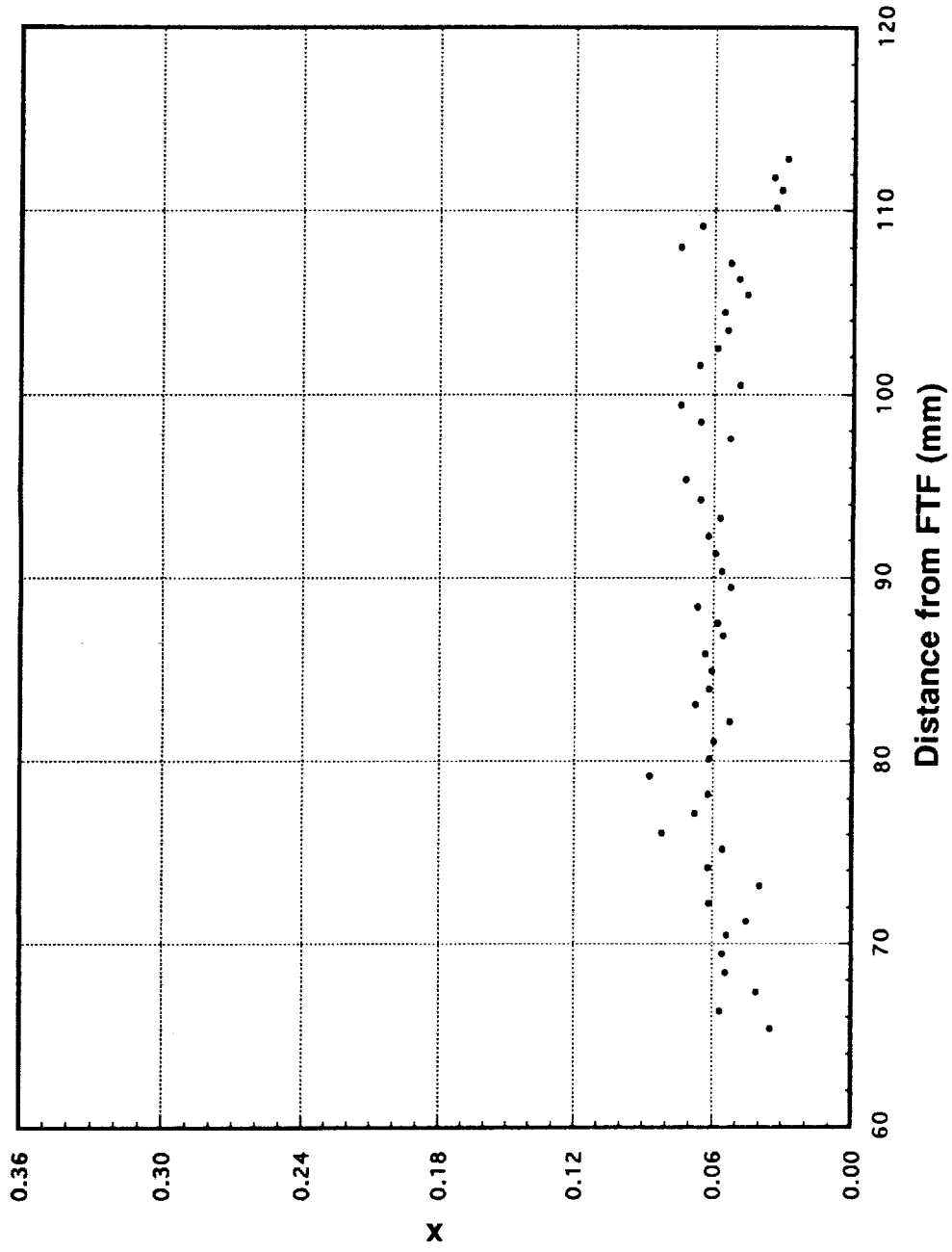


Figure 47 After-anneal off-center-line compositional distribution along the quenched-in portion of the ground truth sample.

B16-34 Ground Truth Sample Quenched HgZnTe  
49 mm from the Interface



Figure 48 Back scattering SEM micrograph of the top portion of the quenched-in part of the ground truth sample.

## *Discussion*

**Question:** *How did you decide where to cut the axial slides? Because the correspondence between the radial segregation profile and the interface morphology I agree is remarkable. How do you decide what angle to cut them ?*

**Answer:** Fortuitous. As a matter of fact, I thought it was truly remarkable and for one thing we never thought we would see non-symmetry. So, when we cut the crystal, we were not sensitive to how exactly to cut. Another interesting thing to note was as you watched the composition evolution, it was rather flat and then started to distort in correspondence to the acceleration data. When you saw the transverse component going in, there is one to one correlation as to how the composition evolved.

**Question:** *The axial (z) acceleration was of the same order as the x component, was it not ?*

**Answer:** Matter of fact, that is the problem. You would like to have the stabilizing gradient to be much larger. In that situation, the axial component will be much larger than the transverse component.

**Question:** *Could you give some estimates of this ratio ?*

**Answer:** As a matter of fact, I am glad you asked that question. Bob Naumann made some estimates on the optimum value. If you do not have any transverse component then you like to have zero axial acceleration but if you have a transverse component of about 0.1 to 0.2  $\mu g$  then you would like to have a drag of 1  $\mu g$  or a little bit more to have a stronger axial stabilizer.

**Question:** *What about the orientation ?*

**Answer:** What you would like to do is to have the primary acceleration axis line up with the sample axis.